9-2007

Flight Dynamic Response of HALE Aircraft to KC-135 Flowfield

Amanda J. Devuono

Flight Dynamic Response of HALE Aircraft to KC-135 Flowfield

THESIS

Amanda J Devuono, 2nd Lieutenant, USAF

AFIT/GAE/ENY-07-S06

DEPARTMENT OF THE AIR FORCE
AIR UNIVERSITY

AIR FORCE INSTITUTE OF TECHNOLOGY

Wright-Patterson Air Force Base, Ohio

The views expressed in this thesis are those of the author and do not reflect the official policy or position of the the United States Air Force, the Department of Defense, or the United States Government.

AFIT/GAE/ENY-07-S06

Flight Dynamic Response of HALE Aircraft to KC-135 Flowfield

THESIS

Presented to the Faculty

Department of Aeronautical and Astronautical Engineering

Graduate School of Engineering and Management

Air Force Institute of Technology

Air University

Air Education and Training Command

In Partial Fulfillment of the Requirements for the

Degree of Master of Science in Aeronautical Engineering

Amanda J Devuono, B.S.

2nd Lieutenant, USAF

September 2007

AFIT/GAE/ENY-07-S06

Flight Dynamic Response of HALE Aircraft to KC-135 Flowfield

Amanda J Devuono, B.S.

2nd Lieutenant, USAF

Approved:

Major Christopher Shearer, Ph.D. (Chairman)	date
Dr. Mark Reeder, Ph.D (Member)	date
Dr. Robert Canfield, Ph.D (Member)	date

Abstract

This research effort examines the static affects of a KC-135 flowfield on a flexible winged Sensorcraft model. The KC-135 flowfield data is generated by a vortex lattice code and integrated into Sensorcraft model for analysis. Building on previous research, a refueling situation was modeled to note the effects of the Sensorcraft at varying locations within the flowfield. The Sensorcraft model was analyzed for both rigid and flexible wings as a means of comparision. Flowfield locations of interest were determined and trimmed conditions were computed for each flowfield location. Utilizing the trimmed condition and flowfield locations, the nonlinear set of EOM's were linearized in order to complete an eigenvalue/eigenvector analysis. Unstable eigenvalues were found for the rigid and flexible cases at all flowfield locations, and the specific contributions to the states were noted and classified accordingly. Results indicate that when the Sensorcraft was moved to different locations, the number and magnitude of the unstable eigenvalues fluctuated. Areas of the flowfield with increases in unstable eigenvalues were determined to be where the Sensorcraft experienced asymmetric loading, primarily when offset from the centerline of the flowfield. The additional elastic states for the flexible winged cases showed a significant increase in unstable eigenvalues.

Acknowledgements

Let me begin by acknowledging that graduate work has been one of the most humbling experiences I have encountered. I have found that the more I learn, I become more and more aware of what there is to learn, and that is just endless. So endless in fact that sleep could be sacrificed for the remainder of my days and still not even scratch the surface. To all those, who aided in my humbling experience. My advisor, who patiently helped me along and refrained from an online auction in many occasions. My husband, who continually reminded me that things can always be much worse, like being in a different service. My Thursday coffee companion, it was rough not being able to yell the coefficient of lift across the room. My family who offered many a encouraging remark and God who held my hand the whole way.

Amanda J Devuono

Table of Contents

Page

Abstract iv

Acknowledgements v

List of Figures viii

List of Tables x

List of Symbols xii

List of Abbreviations xiii

I. Introduction 1

II. Theoretical Development 3
- 2.1 Previous Research and Motivation 3
- 2.2 Very Flexible Winged Aircraft 3
- 2.3 Automated Aerial Refueling Program 6
- 2.4 Wind Tunnel Validation of Vortex Lattice Code 7
- 2.5 Modeling Aircraft in Close Proximity 8
- 2.6 Present Motivation and Problem 9

III. Model Development 10
- 3.1 Coordinate Systems 10
- 3.2 Very Flexible Winged Aircraft Model 12
  - 3.2.1 Rigid Body Equations of Motion 13
  - 3.2.2 Velocity Components as Lift and Moment Contributions 14
  - 3.2.3 Flexible Aircraft Equations of Motion 15
  - 3.2.4 Reference Frames 17
- 3.3 Refueling and Receiver Aircraft Parameters 19
- 3.4 Vortex Lattice Code for KC-135 19
- 3.5 Integration Code for KC-135 data and Receiver Aircraft 21
- 3.6 Orientation of Refueling and Receiver Aircraft within the Flowfield 22
- 3.7 Movement of the Flowfield 22
- 3.8 Trimming Solution 24
  - 3.8.1 Matlab Trimming Routine 24
  - 3.8.2 Newton Raphson Method 25

Page

3.9 Computational Adaptations 26
3.9.1 Trim Calculation - Thrust Elimination 26
3.9.2 Wing Tip Vortices 26
3.10 Final Locations of Aircraft in Flowfield 26
3.11 Linearized A Matrices for the Sensorcraft 28
3.12 Eigenvalue Stability Analysis 29
3.12.1 Longitudinal Motion 30
3.12.2 Lateral Motion 30

IV. Results 32
4.1 Initial Complications 32
4.2 Trimmed Solutions 32
4.3 State Space A Matrices and Eigenvalues 34
4.3.1 Rigid Body Cases 35
4.3.2 Flexible Cases 43
4.3.3 Location $(0, 10)$ 48
4.3.4 Location $(0, -10)$ 48
4.3.5 Location $(10, 10)$ 48
4.3.6 Location $(20, 8)$ 51

V. Conclusions and Recommendations 55
5.1 Conclusions 55
5.2 Recommendations for Future Research 55
5.2.1 Recommendations for the Flowfield Data 55
5.3 Recommendations for Trimming Solution 57
5.4 Recommendations for a Controller 57
5.5 Aircraft Stiffness 58
5.6 General Remarks 58

Appendix A. States for Flexible Model 59

Bibliography 64

List of Figures

Figure		Page
2.1.	Sensorcraft Model	6
2.2.	Testing locations for Wind Tunnel	8
3.1.	Refueling Situation.	11
3.2.	Coordinate Systems.	11
3.3.	Schematic of Modeled Aircraft	12
3.4.	Receiever/B Reference Frame	14
3.5.	Two Dimentional Airfoil	15
3.6.	Local Reference Frame	18
3.7.	Aerodynamic Frame	18
3.8.	Aerodynamic Frame Depiction	19
3.9.	Size Comparison	20
3.10.	Precontact Position.	21
3.11.	W Velocity and Flowfield Comparison	23
3.12.	Small Scale Flowfield	27
3.13.	Large Scale Flowfield	27
3.14.	Locations of Simulation Runs	28
4.1.	Aircraft with Vortex effects	33
4.2.	Wing Deflection	34
4.3.	Rigid Body Cases: Eigenvalues in Complex Plane	36
4.4.	Legend of Location Symbols	36
4.5.	Large Scale View of Dominant Real Eigenvalues	37
4.6.	Large Scale View of Dominant Complex Eigenvalues	39
4.7.	Large Scale View of Intermediate Complex Eigenvalues	41
4.8.	Large Scale View of Dominant Real Eigenvalues	42
4.9.	Large Scale View of Additional Eigenvalues	44

Figure Page

4.10. Flexible Cases: Eigenvalues in Complex Plane 46

4.11. Elastic States 46

List of Tables

Table		Page
3.1.	Key Refueling Aircraft and Receiver Aircraft Specifications	19
3.2.	Initial Control Parameters.	24
4.1.	Trimmed Flight Configurations	36
4.2.	Dominant Real Negative Eigenvalue: Centerline	38
4.3.	Dominant Real Negative Eigenvalue: Offset	38
4.4.	Dominant Complex Eigenvalue: Centerline	39
4.5.	Dominant Complex Eigenvalue: Offset	40
4.6.	Intermediate Complex Eigenvalue: Centerline	41
4.7.	Intermediate Complex Eigenvalue: OffSet	41
4.8.	Least Valued Complex Eigenvalue Pair: Centerline	42
4.9.	Least Valued Complex Eigenvalue Pair: Offset	43
4.10.	Additional Eigenvalues: Centerline	44
4.11.	Additional Eigenvalues: Offset	44
4.12.	No Flowfield- Eigenvalue Pair: 8.6599 (+/-) 93.069i	47
4.13.	No Flowfield- Eigenvalue: .0359	47
4.14.	Location $(0, 10)$ - Eigenvalue Pair: 17.253 (+/-) 173.54i	49
4.15.	Location $(0, 10)$ - Eigenvalue Pair: 67.78 (+/-) 78.964i	49
4.16.	Location $(0, 10)$ - Eigenvalue: 72.077	49
4.17.	Location $(0, -10)$ - Eigenvalue Pair: 270.22 (+/-) 697.6i	50
4.18.	Location $(0, -10)$ - Eigenvalue Pair: 57.415 (+/-) 299037i	50
4.19.	Location $(0, -10)$ - Eigenvalue Pair: 88.174 (+/-) 17.675i	50
4.20.	Location $(0, -10)$ - Eigenvalue: 118.11	52
4.21.	Location $(10, 10)$ - Eigenvalue: 399.27	52
4.22.	Location $(10, 10)$ - Eigenvalue Pair: 12.588 (+/-) 54.43i	53
4.23.	Location $(10, 10)$ - Eigenvalue Pair: 17.214 (+/-) 9.1836i	53

Table Page

4.24. Location $(20, 8)$ - Eigenvalue: .1016 54

4.25. Location $(20, 8)$ - Eigenvalue: .0131 54

A.1. States for Flexible Model 60

A.2. States for Flexible Model (cont.) 61

A.3. States for Flexible Model (cont.) 62

A.4. States for Flexible Model (cont.) 63

List of Symbols

Symbol		Page
v_B	Linear Velocities ($v_{Bx,y,z}$) of the Sensorcraft	13
ω_B	Angular Velocities ($w_{Bx,y,z}$) of the Sensorcraft	13
F	State Dependent External Force	13
M	State Dependent External Moment	13
I	Inertia Matrix	13
ζ	Quaternion Elements	13
p_B	Inertial position of the B reference frame	13
m	Mass of the Sensorcraft	13
b	Semi-chord length of the 2D Airfoil	15
d	Distance from Mid-chord to Beam Reference Line	15
λ_0	Unsteady Inflow Velocity	15
M	Generalized Mass Matrix	16
C	Generalized Damping Matrix	16
K	Generalized Stiffness Matrix	16
R	Generalized Force Vector	16
λ	Finite State Inflow	16
ϵ	Strain	17
θ_B	Orientation of the Receiver Reference Frame	17
U	positive aft	21
V	Velocity in the y direction positive right wing	21
W	Velocity in the z direction positive down	21
α	Angle of Attack	24
δ_e	Elevator Angle	24
$\dot{\theta}$	Pitch Rate	30
$\dot{\psi}$	YawRate	30
$\dot{\phi}$	Roll Rate	30

List of Abbreviations

Abbreviation		Page
UAV	Unmanned Aerial Vehicles	1
DOD	Department of Defense	1
HALE	High Altitude Long Endurance	1
ISR	Intelligence, Surveillance, and Reconnaissance	1
DOF	Degrees of Freedom	3
MLE	Michelob Light Eagle	6
AFRL	Air Force Research Laboratory	6
DARPA	Defense Advanced Research Projects Agency	6
AAR	Automated Aerial Refueling	6
ISR	Intelligence, Surveillance, and Reconnaissance	12
EOM	Equations of Motion	12
EOM	Equations of Motion	13
R.L.	Beam Reference Line	15
L/W	Lift to Weight Ratio	24
LTI	Linear Time Invariant	28

Flight Dynamic Response of HALE Aircraft to KC-135 Flowfield

I. Introduction

Sensorcraft and Unmanned Aerial Vehicle (UAV) research has become increasingly widespread due to the significant contributions to Air Reconnaissance and other Department of Defense (DOD) applications. Regardless of increasing research efforts, there are still many untouched areas which, with an increased knowledge, would aid the warfighter in many applications. Developing more efficient and highly specialized missions for UAV's provides an infinite source of ideas, but a very crucial aspect for unmanned aircraft to emulate manned aircraft is the ability to refuel. Although some research investigates UAV refueling, the majority of the studies have been completed on traditional aircraft models with rigid wings and of very small scale relative to the refueling aircraft. Although this field has not been perfected, there have been significant advances that have enabled successful aircraft to be maneuvered and controlled in a refueling configuration. Developing these types of controllers, however, is similar to existing conventional aircraft with rigid body dynamics. While all of these areas of research support the development of technology that will improve the performance of UAV's and Sensorcraft indirectly, very little has been explored in the realm of other types of aircraft, namely bodies which exhibit nonlinear dynamics and have a wingspan greater than the refueling aircraft. Some recent research directed in modeling high altitude vehicles with flexible wings creates the requirement for more precise and exacting tasks to be possible in order for the UAV's capabilities to mimic piloted flight. Unlike traditional rigid body aircraft, which can be modeled by linear dynamics, these aircraft cannot be characterized as such, and therefore require more complex methods of control. The fact that one of the primary functions of High Altitude Long Endurance (HALE) vehicles is to provide Intelligence, Surveillance, and Reconnaissance (ISR) which almost inherently lends itself to refueling capability, motivates this

research; a preliminary study of the effects of a KC-135 flowfield on a representative HALE aircraft. The goal of this research is to gain a better understanding of the types of instabilities the HALE aircraft will encounter, and, in turn, which areas to avoid as well as the type and magnitude of control needed for the aircraft to remain in a trimmed position in order to successfully be refueled. For this research, analysis is restricted to an aircraft trimmed for longitudinal dynamics and a fixed throttle setting. This is a complex problem with many aspects still untouched, but getting a better understanding of how the aircraft will respond to a dynamic flowfield can help direct future research efforts in order to make refueling a possibility.

II. Theoretical Development

2.1 Previous Research and Motivation

Separately, there are numerous research efforts involving HALE aircraft, UAV's and aerial refueling, but there is still very little that attempts to integrate all three, and a fraction that specifically deals with flexible winged aircraft dynamics. In order to present a better understanding of the problem as a whole, each topic, the challenges it presents, and previous research efforts will be explored.

2.2 Very Flexible Winged Aircraft

Most UAV's that are governed by the classic rigid body EOM's as conventional aircraft can also be controlled using a similar approach as manned aircraft with simulated pilot inputs; this is not the case for flexible winged aircraft. These aircraft do not fall within the bounds of linear motion, they exhibit nonlinear aerodynamic behavior which creates an even greater need to attempt to understand how these aircraft will respond. HALE aircraft characteristics, in general, are commonly indicative of lightweight structures with a fuel fraction of greater than 66 percent, high aspect ratio wings, slender fuselage, and slender control surfaces. The trade off between creating structural rigidity versus a lightweight aircraft is shown, in this case, by the flexible nature of the wings. In recent research by Shearer and Cesnik [10] a flexible aircraft model was developed to investigate the nonlinear effects of the dynamic response of a representative HALE vehicle. The model aircraft, as shown in Figure 2.1, is a simple twin tail configuration with ailerons, rudders, and elevators as control surfaces which was the focus of three types of solutions each with three simulation cases for both heavy and light weight conditions. The solution types included a baseline, with no elastic Degrees of Freedom (DOF) after the wing reaches a steady state deflection (meaning the wings essentially locked into place), a linearized solution utilizing the steady state generalized mass and damping matrices, and a complete nonlinear solution with updated generalized mass and damping matrices at every time step. Beginning each simulation trimming for zero pitching moment about the center of mass,

each of the solution methods were used for for three basic maneuvers. The maneuvers are: simple descending flight, descending flight with elevator input, and descending flight with aileron and rudder input. Comparing the linear and nonlinear solutions for each condition, heavy and light weight, maneuvers that required symmetric loading had similar results for the linear and nonlinear solutions. Conversely, maneuvers requiring asymmetric loading, resulted in a difference between linear and nonlinear solutions, which was further amplified for the heavy weight condition. These findings are particularly important for this research, since refueling deals so closely with weight transfer and asymmetric maneuvering. Specifically, when the aircraft is positioned off the centerline of the refueling aircraft's flowfield, asymmetric loadings on the wing will be encountered. Another aspect not considered in this research, however, is the addition of fuel, essentially meaning a change in HALE Sensorcraft inertia properties, which will create a change in dynamics that cannot be ignored. The importance of having a sound understanding of the nonlinear behavior is necessary for a successful refueling mission.

In an attempt to understand more completely how a controller would need to be designed for a flexible winged aircraft, Shearer and Cesnik [**?**] present a control scheme for trajectory tracking of a flexible winged aircraft based on human pilot operations, both symmetric and asymmetric maneuveris, and for different aircraft loadings. The same Senorcraft model (Figure 2.1) was used for this research. Their analysis was completed using a 6-DOF vehicle dynamics model coupled with elastic DOF based on a strain-based structural formulation for high-aspect ratio lifting surfaces. The controller utilized a fast inner loop for control of the lateral motion using a Linear Quadratic Regulator and a slow outer loop to control the kinematic nonlinearities. Controller performance specifications were set and evaluated for three standard pilot maneuvers: wings level altitude change, steady level turn starting from zero bank angle, and climbing turn. The simulation results from their research concluded that their dual loop architecture was able to track altitude and bank angle changes as-

suming that conditions allowed for smooth air, full elastic state feedback, and perfect sensors. Their findings would possibly, with modifications for dealing with a more dynamic airflow, assist in further research for developing a controller for a refueling operation.

Instability of flexible winged aircraft is a crucial component in the study completed by Patil, Hodges and Cesnik [5]. Their research investigated the aeroelastic instabilities that could constrain the flight envelope for a high aspect ratio wing. Their research was an effort to model the nonlinear behavior of the wings and develop an analysis tool useful for design. Their research highlights the primary problem with modeling nonlinear systems with linearized models: the affect of large disturbances. Linear models are either considered stable or unstable. A flexible model, however, will behave differently depending on the disturbance. Small disturbances will tend to maintain a stable steady state, but greater disturbances could can lead to instability. This supports their findings that varying initial conditions considerably varies the stability of the aircraft. By varying the initial deformation of the wingtip, the aircraft dynamics exhibited stable and unstable oscillations. Flutter instabilities were also considered in this research. Avoiding stall is vital for HALE vehicles which must fly at high trim angles of attack to accommodate the high altitude and slow airspeed condition in which density is a minimum. It was shown that beyond flutter speed for an aircraft, the oscillations will grow but will be counteracted by nonlinear stiffness; essentially meaning that these oscillations will not increase without bound, but will converge to a limit cycle. Analysis of the specific limit cycles could in turn be an indicator of the type of structural forces the aircraft would endure and designs could be modified accordingly so as to prevent failure. Consideration of these findings is applicable to this research where large disturbances of the wing and stall speeds are both possible during a refueling mission

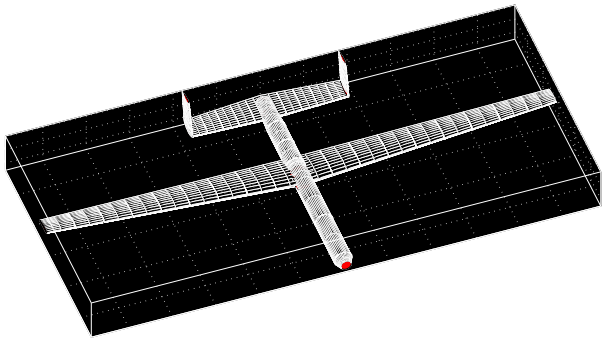

Figure 2.1: Sensorcraft Model

In yet another research effort by van Schoor and von Flotow [8], specifically focusing on the Michelob Light Eagle (MLE), research was conducted to help understand the effects of unsteady airflow and altitude on unstable modes of a flexible aircraft. Using eigenvalue stability analysis, they found that there were substantial variations with airspeed and altitude. To help deal with altitude pressure changes, a proposed static pressure dependent feedback gain could be utilized to develop an adequate controller. This is worth noting for this research, since extreme difference of the normal refueling altitude versus the standard high altitude operating condition of the aircraft will need to be considered for stability throughout a refueling mission.

2.3 Automated Aerial Refueling Program

In recent years, Air Force Research Laboratory (AFRL) and Defense Advanced Research Projects Agency (DARPA) started an initiative to develop a procedure for refueling UAV's. There is an imminent need to have this capability as the Air Force utilizes UAV technology in mission planning. The goal of the Automated Aerial Refueling Program (AAR) is to successfully integrate UAV's into the current military infrastructure [4]. This statement extends to more broad concepts than just refueling, but a preliminary and critical component of any aircrafts' mission capability is

refueling, especially if tasked with extended mission duration, which will be the case with most HALE aircraft. In August of 2006, the Lear Jet was used to validate a controller developed for un-manned refueling and was a success. Although there is much to be learned about the this topic, it was an initial development success.

2.4 Wind Tunnel Validation of Vortex Lattice Code

To aid in the research of the AAR program, there has been significant effort to develop a flowfield model of the KC-135 wake to allow mathematical analysis to be completed. The ability to know specific flowfield parameters is crucial to any sort of research involving refueling and it will aid in the eventual development of a control scheme. That stated, the accuracy of the vortex lattice code used in this research was validated by a series of wind tunnel tests using the Langley Full Scale wind tunnel at Old Dominion University. The results are presented by Blake [1] who concluded that the vortex lattice code gives an accurate estimation of the flowfield a UAV will encounter behind a tanker. The results were particularly accurate for lift and moment calculations and relative magnitudes, but drag calculations varied from predicted. Although not one of the main conclusions of the research, the results also show that there is negligible difference in the strength of the flowfield at varying distances upstream and behind the tanker as shown by Figure 2.2. The distances were measured from the center of gravity of the tanker to the center of gravity of the receiver aircraft. The two test locations behind the tanker were taken at 20 feet and 300 feet aft of the tanker. The negligible difference in flowfield data with longitudinal spacing supports the assumptions of this research which neglects flow variation along the longitudinal direction of the KC-135's flowfield (the distance aft of the aircraft). It was found, however, that there are significant changes in flowfield characteristics in the lateral and vertical directions making it pertinent to model flow variations in these directions for a flexible winged aircraft which will move laterally and vertically within the flowfield depending on the perturbations encountered.

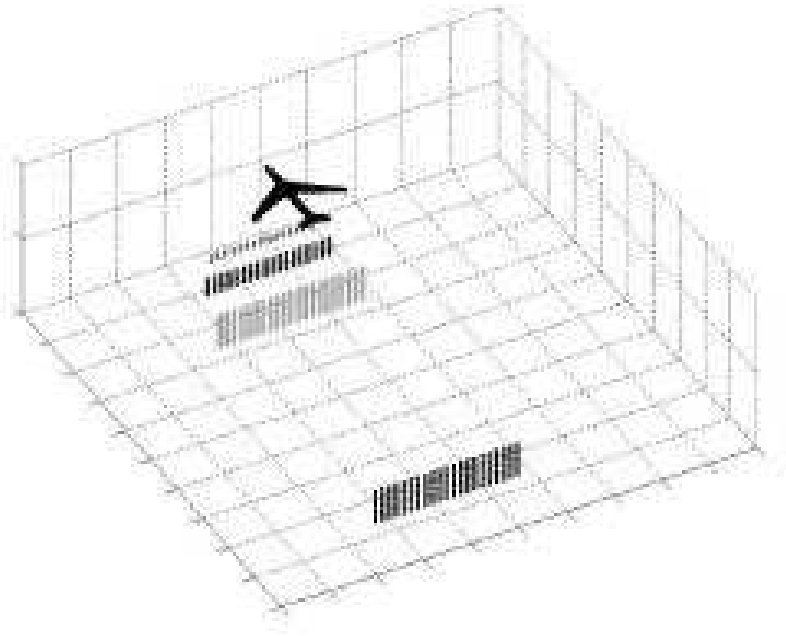

Figure 2.2: Testing locations for Wind Tunnel

2.5 Modeling Aircraft in Close Proximity

Meshing the two areas of research presented thus far, Dogan and Venkataramanan [3] developed a model for the response of an aircraft in close proximity to a refueling aircraft. Their model utilizes a computation of vortex induced wind velocity field and an approximation of nonuniform velocity field by uniform wind components and gradients. This method eliminates the large amounts of data needed for table lookup methods. Their research yielded results which correlated well with wind tunnel validation. Their goal was to provide a good enough match to be able to utilize their findings for further research and development of UAV refueling technology. Their research parallels the primary concern in this research in that the trailing vortex field generated by an aircraft in flight can significantly affect the dynamics of nearby aircraft. That stated, the tankers' vortices can be beneficial in reducing drag/fuel consumed but detrimental to the stability of the receiver aircraft.

2.6 Present Motivation and Problem

This research combines a flexible Sensorcraft model and a KC-135 flowfield data in a refueling situation in order to be able to analyze the effects a flowfield will have on a Sensorcraft. The primary difference that sets this research apart from others presented is the flexible nature of the aircraft wings. The effect of the flowfield from the tanker becomes even more difficult to model because the flexibility of the wings places different locations on the wings in different areas of the KC-135's flowfield, which have already been discussed as varying with lateral and vertical location. This complicates making an accurate model of the forces and moments the wings are experiencing, but in turn makes it even more crucial for the eventual development of an adequate control scheme for such aircraft. In order to optimize the position the Sensorcraft flies behind the KC-135 during refueling, and which areas that should be avoided, there is a need to simulate the Sensorcraft's behavior when subjected to the forces generated by the flowfield of a KC-135 in varying refueling flight configurations. Determining possible areas of instability for the flexible winged Sensorcraft will aid in future research and development of a controller adequate for successfully completing a refueling mission.

III. Model Development

In order to integrate the flowfield and receiver aircraft model together, a description will be offered of each and then further explained in context specific to this research. The first and primary source is the model of a HALE Sensorcraft designed by Shearer and Cesnik [?, 10] which was triggered by the growing importance of HALE aircraft to both the military and civilian communities. The second crucial piece of research is the KC-135 flow-field model data generated by Blake [1] which tabulates flow-field velocities behind a KC-135 using vortex lattice code. Meshing these two models, a theoretical refueling situation was designed to simulate the types of flow that the HALE Sensorcraft will encounter when located behind the KC-135. This situation is depicted in Figure 3.1. Stability analysis can then be conducted to determine acceptable areas behind the tanker where stability is maintained. To clarify which aircraft is being referenced, the Sensorcraft will be referred to as the receiver aircraft and KC-135 as the refueling aircraft for the remainder of the model development.

3.1 Coordinate Systems

Clarification of the coordinate systems is necessary since the flowfield and receiver aircraft conventions are different. For the purposes of this research the coordinate system used will be the receiver aircraft convention. These are depicted in Figure 3.2. The tanker flowfield data utilizes x positive aft, y positive out the right wing, and z positive up. The Sensorcraft model utilizes x positive out the right wing, y positive out the nose, and z positive up. Coordinate transformations from the flowfield convention to the receiver aircraft were completed in the flowfield interpolation code which will be explained in section 3.5. Further transformations will be required in the development of the refueling situation, but will be addressed in the particular sections as needed.

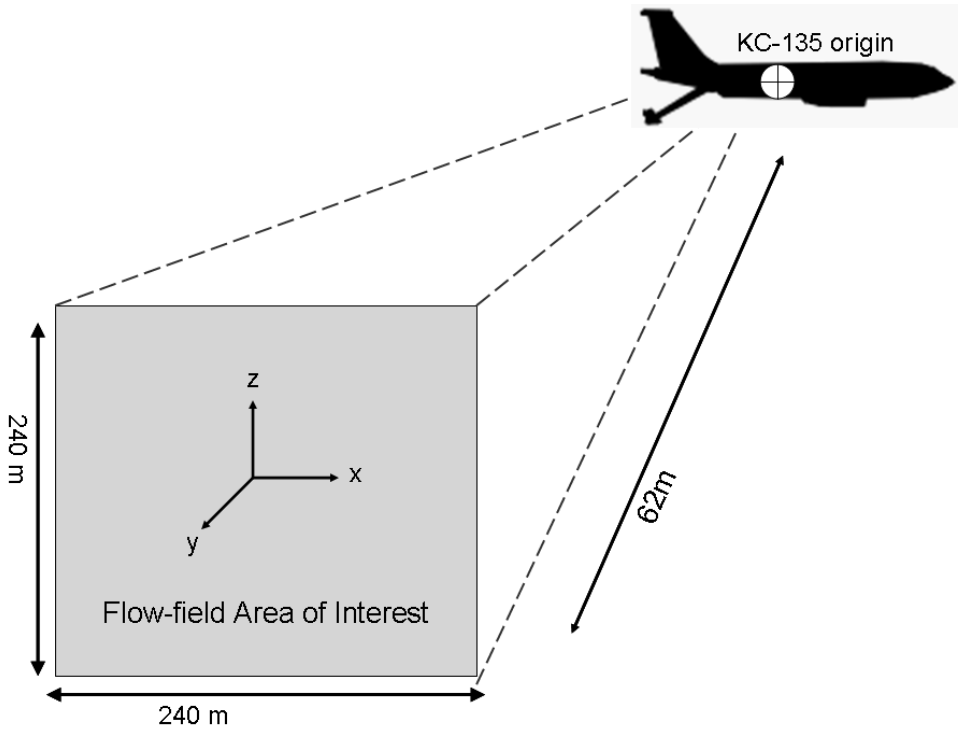

Figure 3.1: Refueling Situation.

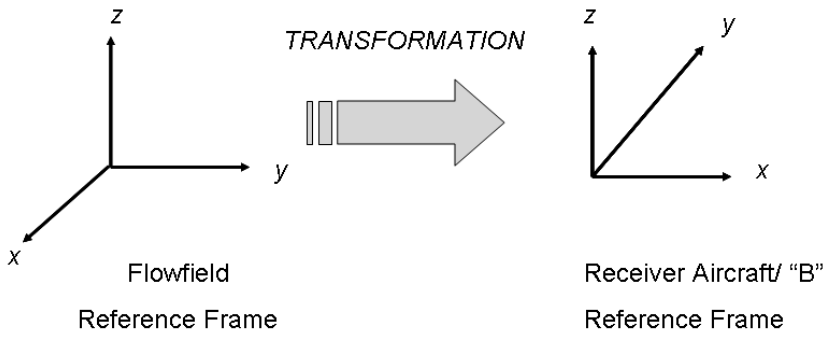

Figure 3.2: Coordinate Systems.

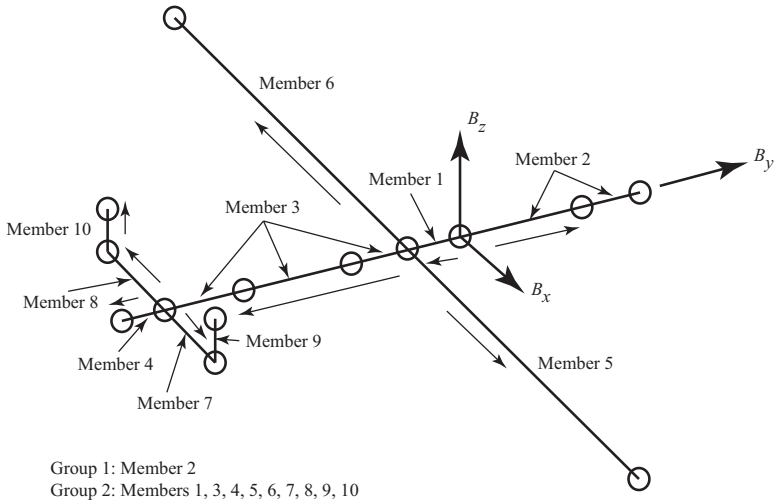

Figure 3.3: Schematic of Modeled Aircraft

3.2 Very Flexible Winged Aircraft Model

The very flexible aircraft referenced in the work of Shearer and Cesnik [?] was designed with the intention of creating a very light weight and slender winged endurance aircraft. Typical application for this type of aircraft can be narrowed to three primary missions: airborne Intelligence, Surveillance, and Reconnaissance (ISR), network communication nodes, and general atmospheric research. Inherently, because of the nature of this type of structure, compromising rigidity for weight results in wings that will deform beyond linear geometric displacement assumptions during flight. The movement of the wings can be predicted to some degree so as to design a wing to be able to endure the types of loading it will encounter, but control presents a significant problem in addition. For this research, as a means of comparison, a rigid body model and a flexible winged model were used as developed by Shearer and Cesnik [10]. More exacting development of the equations of motion (EOM) for the rigid and flexible cases can be found in Reference [10]. Figure 3.3 is a schematic of how the aircraft is divided into members. Members are further divided into finite elements which utilize the finite strain approach [2,9]. Internal to the code the user can specify which members are flexible and rigid. The members considered to be flexible for this research are 5 and 6, the aircraft wings.

3.2.1 Rigid Body Equations of Motion. Propagation of the rigid body states of the receiver aircraft reference frame, which is depicted in Figure 3.4 as the B reference frame, in which the first order differential equations, in general, are defined as

$$\dot{x} = f(x, u) \tag{3.1}$$

where x represents the states of the receiver aircraft or B reference frame, and u represents the control inputs. For this research since a static steady state solution was used, there are no control inputs, only an initial trimmed parameter for the elevator which was the only control surface considered. More specifically for the rigid body formulation of the Sensorcraft model the equations of motion (EOM) are shown in Equation 3.2:

$$\begin{aligned} \dot{v}_B &= f_v(v_B, \omega_B, \zeta, p_B, G_0', m, F) \\ \dot{\omega}_B &= f_\omega(\omega_B, I, \zeta, p_B, M) \\ \dot{\zeta} &= f_\zeta(\zeta) \\ \dot{p}_B &= f_p(\zeta, v_B) \end{aligned} \tag{3.2}$$

where v_B and ω_B are the linear and angular velocity variables of the receiver aircraft reference frame (B reference frame); F and M are the state dependent external forces and moment; m is the Sensorcraft mass and I is the inertia matrix of the aircraft. The ζ term is a vector of quaternion elements for determination of the orientation of the receiver/B reference frame and p_B is the inertial position of the receiver/B reference frame. There are some parameters worth highlighting here as they will change for the flexible cases in which the wings are not locked into place. The mass of the Sensorcraft (m) will change depending on fuel loss or gain. The fuel change is not modeled in this research but would be necessary to consider in later efforts. The F term which will be formulated as a lift force on the wing, will change with varying velocity components and with geometry changes of the aircraft. The I matrix will change as the inertia properties of the aircraft vary as the wings flex. Finally, the M term will change as the location in the flowfield changes and with geometry changes of the Sensorcraft. There are three key assumptions also defined in the work of Shearer and Cesnik [10]

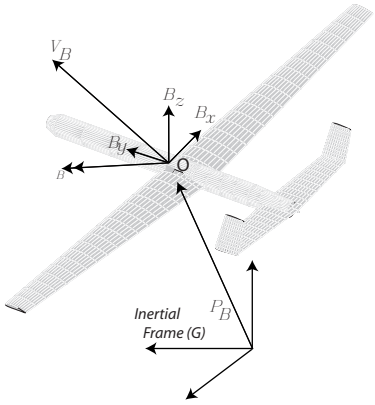

Figure 3.4: Receiever/B Reference Frame

which are essential for the rigid body development and are not considered for the flexible wing . They are: 1) inertia properties are constant or slowly time varying, 2) the inertial force obtained from the cross of the aircraft's angular velocity and the relative velocity of the flexible members is inconsequential and finally, 3) F and M, the external forces and moments as a result of the aerodynamic loading are based on a fixed aircraft geometry.

3.2.2 Velocity Components as Lift and Moment Contributions. In order to compute the steady and unsteady forces and moments for the Sensorcraft model the finite state strain theory used by Shearer and Cesnik [10] from the work of Peters and co-workers [6, 7] will be used. The theory was developed for a two dimensional thin airfoil operating in an inviscid and incompressible flow. The lift, L^{aero} and the moment, M^{aero} about the beam reference line are given by Equations 3.3 and 3.4

$$L^{aero} = 2\pi\rho b(-\dot{y}\dot{z} + (b-d)\dot{y}\dot{\alpha} - \dot{y}\lambda_0 - \frac{1}{2}b\ddot{z} - \frac{1}{2}bd\ddot{\alpha}) \tag{3.3}$$

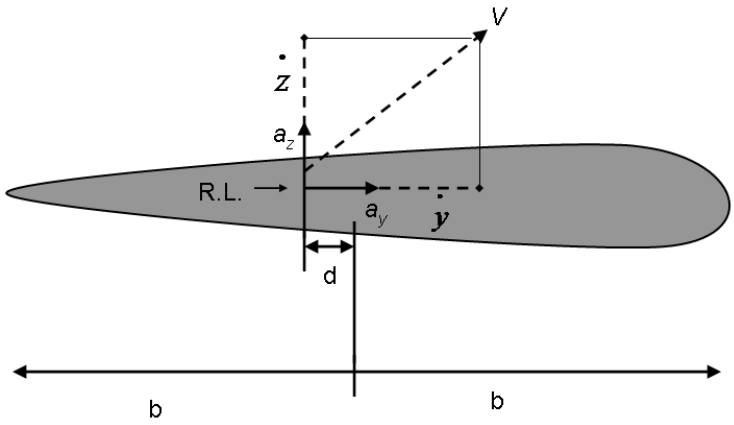

Figure 3.5: Two Dimentional Airfoil

$$M^{aero} = dL^{aero} + 2\pi\rho b^2(-\frac{1}{2}\dot{y}\dot{z} - \frac{1}{2}d\dot{y}\dot{\alpha} - \frac{1}{2}\dot{y}\lambda_0 - \frac{1}{16}b^2\ddot{\alpha}) \tag{3.4}$$

where b is the semichord length and d is the distance from the mid-chord to the beam reference line (R.L.), Figure 3.5. The $\dot{y}$ and $\dot{z}$ terms are the velocity components along the chord and perpendicular to the chord respectively. For the purposes of this research the $\ddot{z}$ and $\ddot{\alpha}$ terms will be neglected because static solutions are computed. The aircraft is in a fixed position where the wings are able to deflect. There will also be no unsteady inflow velocity term (λ_0) because a steady state static solution is computed. Refining Equations 3.3 and 3.4 yields Equations 3.5 and 3.6 show the most important variables of interest for this research. Namely, the $\dot{y}$ and $\dot{z}$ terms which will vary significantly throughout the flowfield.

$$L^{aero} = 2\pi\rho b(-\dot{y}\dot{z} + (b-d)\dot{y}\dot{\alpha} \tag{3.5}$$

$$M^{aero} = dL^{aero} + 2\pi\rho b^2(-\frac{1}{2}\dot{y}\dot{z}) \tag{3.6}$$

3.2.3 Flexible Aircraft Equations of Motion . The development of the flexible equations of motion is significantly more involved than the rigid body formulation

because of the added states. The lift and moment computed by Equations 3.3 and 3.4 are incorporated into a generalized force vector, R, as shown in equation 3.7 to be used in the flexible EOM's.

$$R = \begin{bmatrix} R_F \\ R_B \end{bmatrix} \tag{3.7}$$

The general form of the coupled rigid body and elastic EOM's is given by Equation 3.8. More detailed development of the elastic EOM's is in the work of Shearer and Cesnik [10].

$$\begin{aligned} M_{FF}\ddot{\epsilon} &= -M_{FB}\dot{\beta} - C_{FF}\dot{\epsilon} - C_{FB}\beta - K_{FF}\epsilon + R_F \\ M_{BB}\dot{\beta} &= -M_{BF}\ddot{\epsilon} - C_{BB}\beta - C_{BF}\epsilon + R_B \\ \dot{\zeta} &= -\tfrac{1}{2}\Omega_\zeta \zeta \\ \dot{p}_B &= \left[C^{BG}0\right]\beta \\ \dot{\lambda} &= F_1\ddot{q} + F_2\dot{q} + F_3\lambda \end{aligned} \tag{3.8}$$

where

$$\beta = \begin{bmatrix} v_B \\ \omega_B \end{bmatrix} \tag{3.9}$$

$$q = \begin{bmatrix} \epsilon \\ p_B \\ \theta_B \end{bmatrix} \dot{q} = \begin{bmatrix} \dot{\epsilon} \\ v_B \\ \omega_B \end{bmatrix} \ddot{q} = \begin{bmatrix} \ddot{\epsilon} \\ \dot{v}_B \\ \dot{\omega}_B \end{bmatrix} \tag{3.10}$$

In Equation 3.8, the M, C, and K are the assembled generalized mass, damping and stiffness matrices, respectively. R is the generalized force vector (Equation 3.7) which contains the lift and moment computed by the finite state aerodynamic model (Equations 3.3 and 3.4) and are a function of the finite state inflow (λ). The β term shown in Equation 3.9 and seen in Figure 3.4 represents the linear and angular velocities of the Sensorcraft. The ϵ and $\dot{\epsilon}$ terms are the strain and strain rate states, respectively. The states represented by q (Equation 3.10) are a set of generalized

coordinates for strain (ϵ), inertial position (p_B), and the orientation of the receiver/B reference frame (θ_B). The state dependence of M, C, and R matrices allows for coupling of the rigid body and flexible dynamics. The initial development of the nonlinear elastic EOM was completed in several steps to capture the virtual work for rigid bodies and flexible slender beam structures, the kinematic relationship between the beam dependent position vectors and the corresponding strains, and finally the summation of the EOM's required further transformation from a set of dependent position vectors and nonminimum set of B reference frame components to an independent set of strain and both linear and angular body velocity and acceleration variables. As a final step to account for the B reference frame orientation and displacement, a set of quaternions and inertial position differential equations were appended [10]. For the purposes of this research the flexible EOM's can be further simplified from Equations shown in 3.11 to a more specific set as shown by 3.11. Note that the acceleration terms cancel from the equation because a steady state static solution is computed.

$$\begin{aligned} C_{FB}\beta + K_{FF}\epsilon &= R_F \\ C_{BB}\beta + C_{BF}\epsilon &= R_B \\ \dot{\zeta} &= -\tfrac{1}{2}\Omega_\zeta \zeta \\ \dot{p}_B &= \left[C^{BG}0\right]\beta \\ \dot{\lambda} &= F_1\ddot{q} + F_2\dot{q} + F_3\lambda \end{aligned} \tag{3.11}$$

3.2.4 Reference Frames. The reference frames as mentioned in the mathematical development and depicted in Figures 3.6 and 3.7 illustrate the transformations from the inertial frame to the aerodynamic frame. To rotate a tanker aircraft flowfield velocity into the appropriate reference frame for aerodynamic calculation, it is necessary to first rotate from G inertial reference frame, to the body fixed B reference frame. The B frame is centered on point O, which is not the aircraft's center of mass (Figure 3.4). From the B frame, a transformation to the local elastic frame at the specific points of interest. The points of interest are denoted by (w_x, w_y, w_z) and can be considered to be anywhere along wing. Shown in Figure 3.7 is the rotation

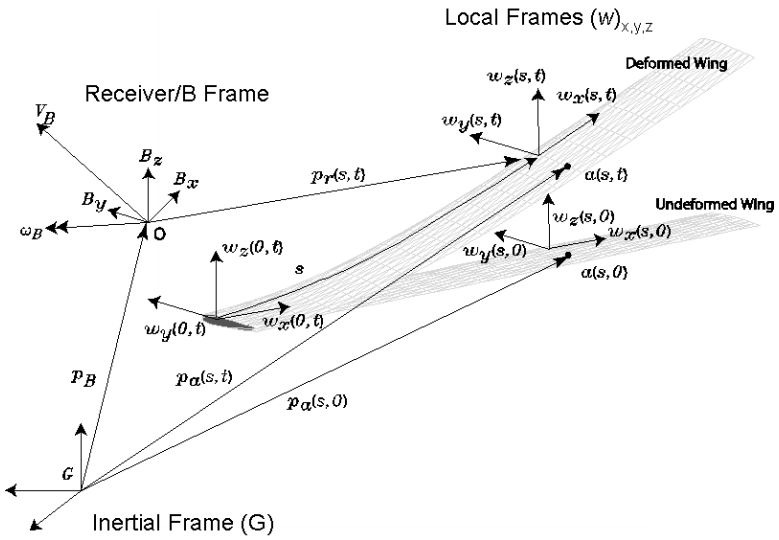

Figure 3.6: Local Reference Frame

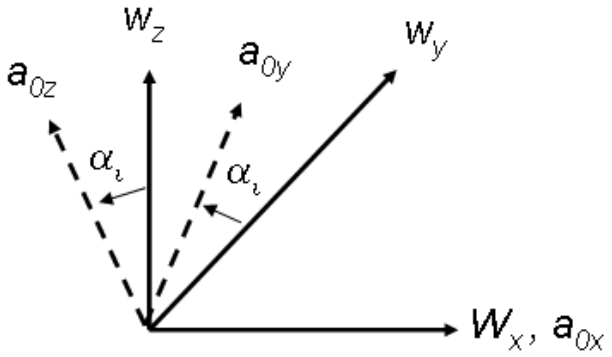

Figure 3.7: Aerodynamic Frame

from the local elastic frame to the aerodynamic frame which is dependent on angle of attack, α. The account for the zero lift angle of attack which we be a function or the wing design.Figure 3.8 shows a swept and unswept wing case. The aerodynamic frame is denoted as the a_0 axis which remains perpendicular to the longitudinal axis of the aircraft. The w_x and a_0 values are shown to be the same for the unswept wing and offset for the swept case. Since the aircraft of interest in this research does not have sweep, the w_x and a_0 will be aligned.

(a) Unswept Wing (b) Swept Wing

Figure 3.8: Aerodynamic Frame Depiction

Table 3.1: Key Refueling Aircraft and Receiver Aircraft Specifications

Aircraft	Refueling Aircraft	Receiver Aircraft
Wingspan	39.9 m	58.6 m
Length	41.53 m	26.4 m
Weight	136,000kg	32,000 kg

3.3 Refueling and Receiver Aircraft Parameters

To aid in understanding of this research, it is applicable to discuss the relative size comparisons of the receiver aircraft and the refueling aircraft. Figure 3.9 and Table 3.1 help present this information. The wingspan of the Sensorcraft will extend to almost 20 meters beyond that of the KC-135, however the length is considerably shorter. The minimal weight and volume of the Sensorcraft is merely a fraction of the KC-135 weight (fully loaded) volume. This allows the assumption for this research to be made that there is little affect from the Sensorcraft on the KC-135 flowfield.

3.4 Vortex Lattice Code for KC-135

The vortex lattice code developed by Blake [1] was modified to interface with the HALE Sensorcraft, since specifications can be modified in the code specific to the receiver aircraft. The flowfield velocities were determined for several KC-135 weights for an altitude of 30,000 ft with a true airspeed of 607.5$\frac{ft}{sec}$. This flight condition is considered to be in the upper portion for altitude and lowest portion for speed within the KC-135 refueling envelope. This was ideal for the Sensorcraft which will have speed limitations and be designed for high altitudes. To examine worst case scenario,

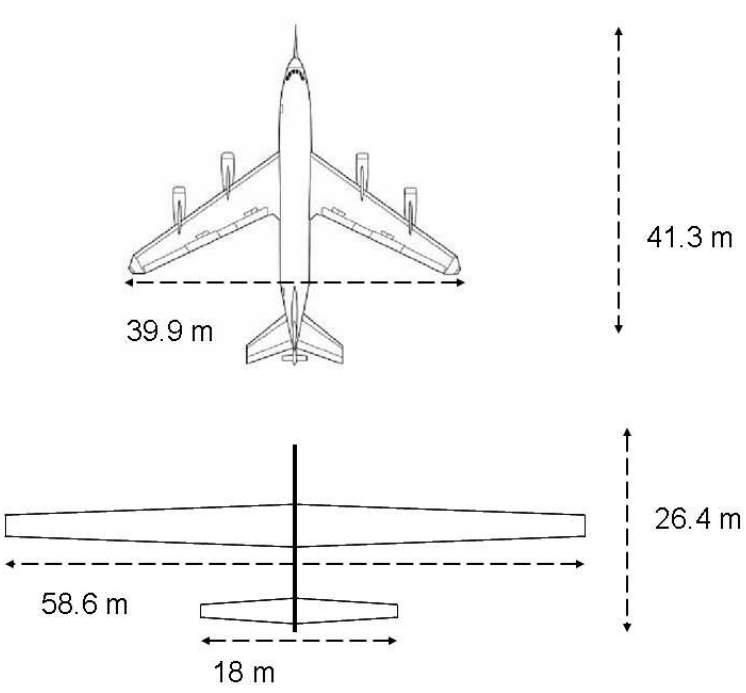

Figure 3.9: Size Comparison

where flowfield velocities are more intense, the code for the heaviest configuration was used at 300,000 pounds. The format of the data from the Vortex Lattice Code consisted of 8 variables. These are the x, y, and z coordinates of the location in the flowfield, the incremental u, v,and w velocity components at the specific location and the local angle of attack and sidewash in degrees. These values were calculated over a 240 meter square area, with 1 meter spacing. This area exceeds the dimensions of the Sensorcraft in order to ensure the full aircraft is subjected to the flowfield. The origin of the flowfield is simulated to represent the actual refueling pre-contact position as shown in Figure 3.10. Solely for the flowfield data, the coordinate system is defined as x positive aft, y coordinate positive out the right wing and z positive up. This is mentioned simply to ensure that later research is consistent. The distance behind the tanker is fixed at pre-contact position which is 15 meters aft of the boom, and a total of 62 meters aft of the origin of the KC-135 coordinate system at the center of gravity. Variation of flow velocities in the x direction were considered to be negligible [1] and therefore neglected for computational efficiency .

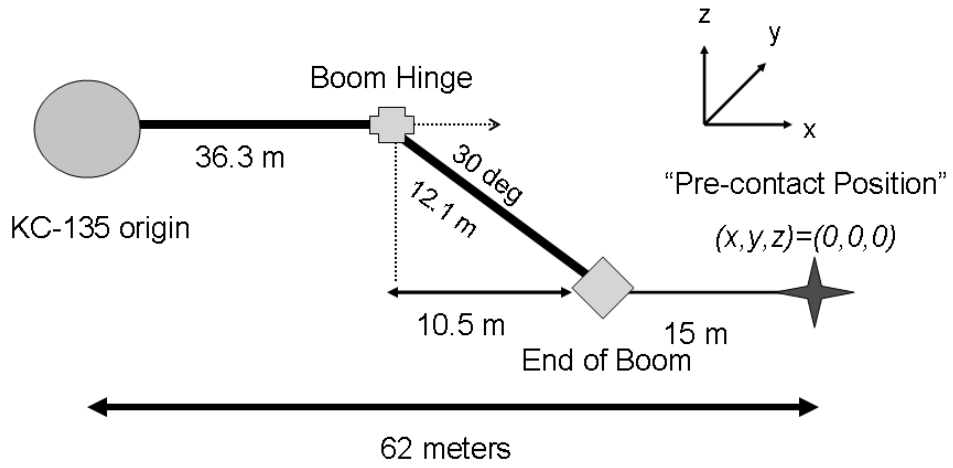

Figure 3.10: Precontact Position.

3.5 Integration Code for KC-135 data and Receiver Aircraft

In order to integrate the tabular flowfield data and the receiver aircraft model, velocities at any particular point in the flowfield were needed. These velocities are then used to calculate the aerodynamic forces and moments (Equations 3.3 and 3.4) along the wing. Due to the flexibility of the wing, from one location to the next, there can be significant position changes, and therefore significant velocity changes. To model this correctly, the tabular flowfield data was imported into a Matlab script to interpolate between the originally 1 meter spaced values. A splining method was used to generate intermediate values at more precise locations in order to generate velocity in the x direction (U), velocity in the y direction (V) and velocity in the z direction (W). Note that there was no velocity variation in the longitudinal direction. Matlab's spline command was used to create a vector of new flowfield velocities with 0.01 meter spacing and the *dsearchn* command was used to find the index of the nearest location for a given coordinate. In order to utilize the velocity values it was essential for those velocities to be rotated into the B reference frame, which is fixed to the point at leading edge of the wing for this model and shown in Figure 3.4. Further development is found in Shearer and Cesnik [10]. For this research the lateral and vertical velocity components were the only ones considered. A final rotation from the

B reference frame into the aerodynamic frame allows for lift and moment calculation as explained in Section 3.2.3.

3.6 Orientation of Refueling and Receiver Aircraft within the Flowfield

The Sensorcraft flies in the plane fixed for the y coordinate at the pre-contact position where the x and z coordinates are zero, and therefore in the middle of the 240 meter flowfield area (note sensorcraft reference frame is:x positive out the right wing and y positive aft along the fuselage). It can be assumed that there is negligible variation along the longitudinal (y) axis as explained by the work of Blake [1]. As shown in Figure 3.11, the vertical, W, velocity along the x axis of the flowfield plane reveals that there are strong downward velocities where x is zero due to the effects of the vortex swirling. The effects of the vortices themselves are seen where x is 20 meters in either direction from the origin. The w velocity begins to change from negative to positive between 7 and 28 meters very rapidly which should be the case since the vortex is centered at 20 meters. Dissipation of the flowfield beyond the 28 meter x locations can also be seen along the x axis in either direction of the flowfield area.

3.7 Movement of the Flowfield

In order to investigate the effects of the KC-135 flowfield on the receiver aircraft it was necessary to be able to move the location of the receiver aircraft within the flowfield. This was simulated by moving the flowfield around the receiver aircraft essentially by adding position coordinates to each of the aircraft members, the new position of the aircraft wings corresponding to a new velocity at a different location in the flowfield. The position can be varied by a user defined variable in the Matlab script which will be explained in the following section for the trimming routine.

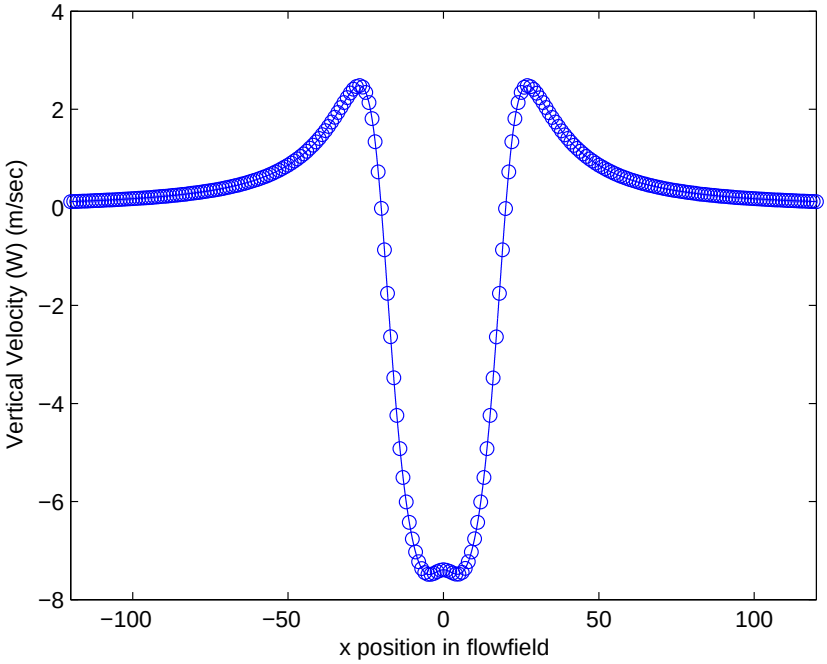

(a) W Velocity Along Wing at Center of Flowfield

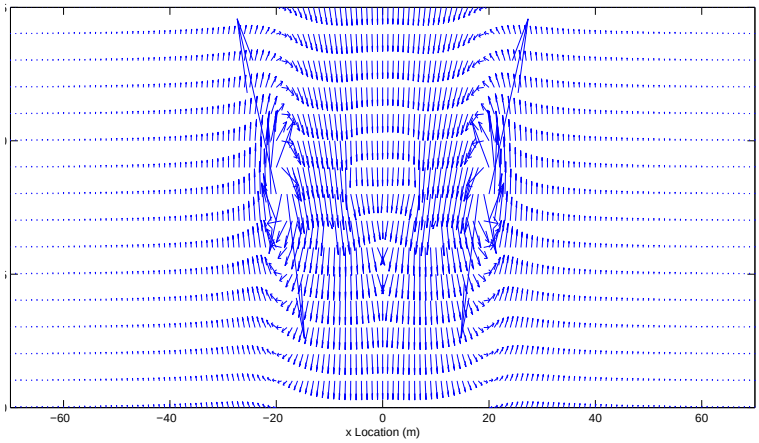

(b) Flowfield View

Figure 3.11: W Velocity and Flowfield Comparison

Table 3.2: Initial Control Parameters.

Control Parameter	Initial Guess
α	1.81 deg
δ_e	3.87 deg
Thrust	83,135 lbs

3.8 Trimming Solution

In order to realize if flight with reasonable control parameters is achievable, a model combining the Sensorcraft/receiver aircraft model, the KC-135 flowfield data, and integration code enables this analysis. A common technique of iteration, the Newton Raphson Method, is used to solve for the trimmed solution of the receiver aircraft at varying locations within the flowfield.

3.8.1 Matlab Trimming Routine. A Matlab routine originally developed by the work of Shearer [9], and modified to support the work of this research, was utilized to compute the necessary angle of attack and elevator angles for Straight and Level Flight: lift to weight ratio (L/W) and pitching moment of zero. These trimmed conditions at the different areas within the flowfield can also be thought of as the equilibrium condition for the particular location in the flowfield. This concept becomes more applicable in the eigenvalue stability analysis presented in Section 3.12. This is a very simple solution that does not include any aileron or rudder inputs which will lend itself to further research. The code begins with a set of initial control input parameters for the Angle of Attack (α), Elevator Angle (δ_e) and the thrust. The initial parameters for these simulations are noted in the Table 3.2.

Beyond defining the initial aircraft parameters, the flowfield parameters are also input in this routine. The position in the x and z directions are defined for the desired position in the flowfield. The specific locations are defined later on.
The mathematical development of the cost function for the trimming solution is defined by

$$J_{trim} = f^T * f \tag{3.12}$$

where for this case

$$f = \begin{bmatrix} \dot{v}_{Bz} \\ \dot{w}_{Bx} \end{bmatrix} \tag{3.13}$$

This cost function is minimized for the solution space using δ_e and α. The Newton Raphson method is then used to propagate the solution process.

3.8.2 Newton Raphson Method. The Newton Raphson method is a common method for solving equations to find a zero valued solution, $f(x) = 0$. The elementary nature and rapid computational speed of the method is an ideal match for this research. The basic premise of the method involves the approximation of a function using tangents. An initial approximation is a key element in this computational method as a more accurate guess will decrease the number of iterations and therefore computational time. Specific to this research, a local minimum of the search variables (δ_e and α) is computed as represented by the following

$$\Delta S_k = \left[\frac{\delta f}{\delta S}\right]_k^{-1} f_k \tag{3.14}$$

where

$$S_k = \begin{bmatrix} \delta_e \\ \alpha \end{bmatrix}_k \tag{3.15}$$

and is then propagated by Equation 3.16 where ΔS is specific to each of the search variables

$$S_{k+1} = S_k + \Delta S \tag{3.16}$$

The Newton Raphson iteration process obtains a solution for trimmed search variables when reaching a user defined tolerance.

3.9 Computational Adaptations

3.9.1 Trim Calculation - Thrust Elimination. The thrust search variable was eliminated for the trim calculation in the Newton Raphson search since it does not have a significant effect on the pitching moment and vertical force. For these cases analyzed, the aircraft is assumed to be in a fixed position, but the wing is able to deflect. This enables the trimmed solution to be computed without thrust variables. In the interest of efficiency, for the simulation, this streamlined calculation was thus preformed. This modification to the original routine was described in the previous section, however, it is noted here since it could be included in further research when the aircraft is not in a fixed position.

3.9.2 Wing Tip Vortices. Preliminary computations exhibited extreme fluctuations in flow velocities along the receiver aircraft wing which inhibited a trim solution for the angle of attack and elevator. A view of the flowfield shown in Figure 3.12 helps illustrate the magnitude of the velocities in the vortex relative to nearby velocities. The large fluctuations were due to the vortex model of the wing tip vortices from the KC-135 flowfield model. These vertical, W, velocities alone were as large as 70 m/s near the vortex as compared to only a few meters outside of the vortex center where velocities decrease rapidly to 10 m/s and dissipate further with distance. Figure 3.13 illustrates the symmetry of the flowfield velocities with vortices centered around the $(20, 8)$ and $(-20, 8)$ locations for (x, z). For the purposes of this research, these areas will be avoided and the receiver aircraft will be placed at locations where the wing will not be subjected to these extreme velocities that prevent convergence of the trim solution.

3.10 Final Locations of Aircraft in Flowfield

Due to the complications of the singularity of the the vortex in the flowfield, areas to examine the receiver aircraft were not determined until initial simulations showed convergence at specific points. To gain an adequate understanding of how

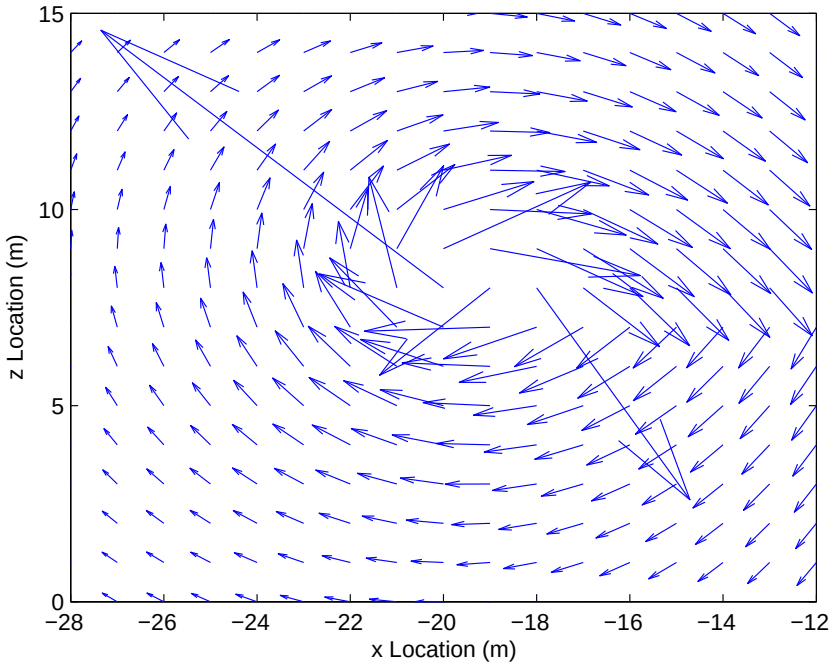

Figure 3.12: Small Scale Flowfield

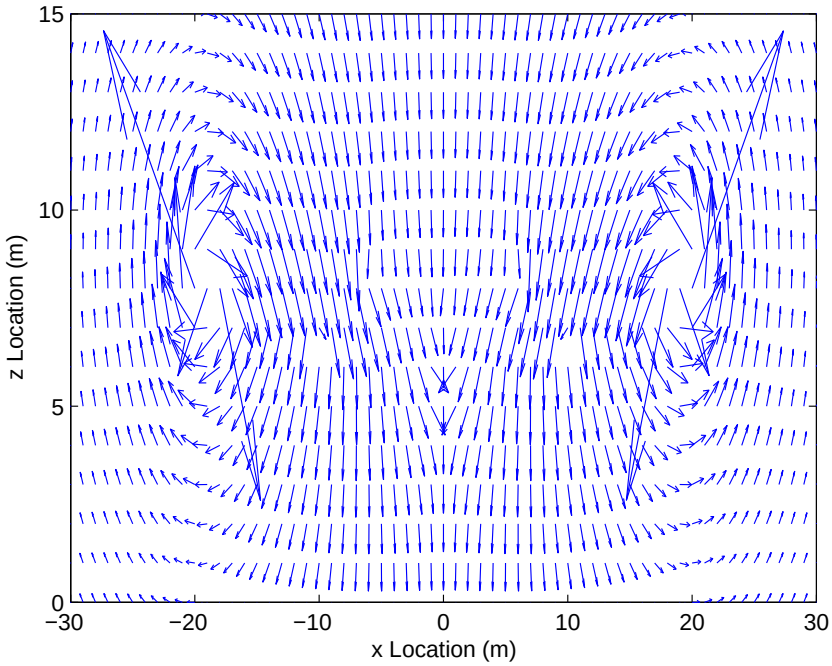

Figure 3.13: Large Scale Flowfield

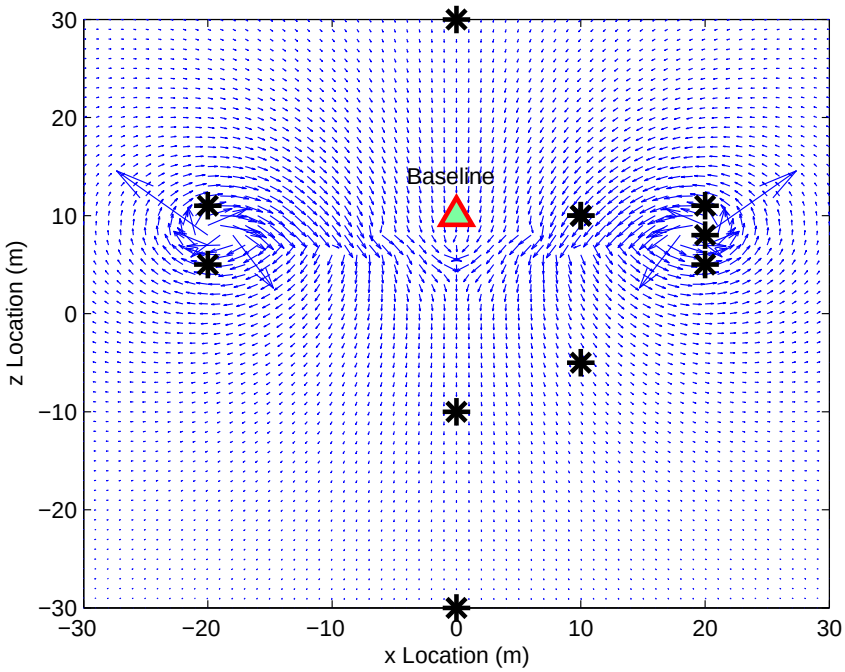

Figure 3.14: Locations of Simulation Runs

the receiver aircraft will behave with the effects of the flowfield, strategic locations to compute the trimmed parameters for further analysis were chosen. Key locations of receiver aircraft placement in the flowfield were chosen as depicted by Figure 3.14 and listed in Table 3.10. Simulations at each location were examined for the aircraft with a rigid body as well as flexible wings as a means to compare results. Note that in all cases where the term no flow is referenced, it means that there is the absence of the KC-135 flowfield.

3.11 Linearized A Matrices for the Sensorcraft

Using the final converged angle of attack, elevator angle and constant thrust, a Matlab routine to solve the nonlinear first and second order differential EOM's (Eq. 3.8) and obtain the Linear Time Invariant (LTI) A state space matrices for the receiver aircraft when subjected to the KC-135 flowfield was used [11]. This routine perturbs each of the states a percentage of their current value and evaluates the new

Test	(x, z) location
Baseline	$(0, 10)$
1	(0,30)
2	(0,-10)
3	(0,-30)
4	(20,11)
5	(20,5)
6	(-20,11)
7	(-20,5)
8	(10,-5)
9	(10,10)
10	middle vortex

states based on the perturbation to formulate the A matrix of the system. Stability can then be analyzed based on the eigenvalues of the system. The LTI system is represented as

$$\dot{x} = f(x) = Ax \tag{3.17}$$

where

$$x = \begin{bmatrix} \epsilon \\ \dot{\epsilon} \\ \beta \end{bmatrix} \tag{3.18}$$

3.12 Eigenvalue Stability Analysis

Using the A matrices generated from the Matlab routine, the eigenvalues are computed to analyze the stability of the system in the various configurations simulated. By convention, eigenvalues in the left half plane are considered stable, thus negative real values are desirable. By contrast, eigenvalues that have positive real values are considered to be unstable. Eigenvalues with complex values are considered to be oscillatory and their stability is then based on the real portion. For this research analysis, the rigid and flexible cases in different areas of the flowfield are examined. The eigenvalues which migrate into the left half plane with flowfield location change are noted, as well as further classification to specific dynamic modes of motion will be presented. For the flexible cases, the method must be modified slightly since the

modes of motion are not traditional. Classification of the unstable modes can then be determined. Modes that pose the greatest threat to overall instability of the aircraft would need to be addressed in control development. A brief summary of aircraft modes of motion will be offered as a precursor to results interpretation. The motion of an aircraft is generally categorized in two groups, lateral and longitudinal. Longitudinal components are the v_y and v_z velocities and the pitching rate, $\dot{\theta}$. Lateral components are the yaw rate, $\dot{\psi}$, roll rate, $\dot{\phi}$, and the v_x velocity. When perturbed, an aircraft can exhibit unstable oscillatory or divergent modes of motion.

3.12.1 Longitudinal Motion. There are two oscillatory modes of motion for the longitudinal motion of the aircraft, Phugoid and Short Period. Phugoid is lightly damped and has a long period, with motion characterized by change in pitch attitude and forward speed. Changes in pitch rate and angle of attack are minimal. The short period mode, in contrast, is heavily damped and has a short period, with motion characterized by change in angle of attack and pitch rate. Changes in forward speed are minimal. The vertical motion is very minimal in this mode. Of these modes, the short period mode is of considerable importance to this research because of the stability implications. Because of the high frequency of the mode, in order for an aircraft to maintain stability when perturbed, it must be heavily damped. This ensures the aircraft will respond to a commanded elevator input. Light damping would present a control dilemma, and the aircraft would be more challenging to control. The Phugoid mode, because of its low frequency, can be more easily controlled and therefore is less of a threat to instability. Another consideration specific to this research is the change in the longitudinal modes with varying center of gravity. The flexible wings of the Sensorcraft will be continually changing center of mass as it encounters forces on its' wings.

3.12.2 Lateral Motion. There are two modes of motion for the lateral motion of an aircraft, spiral and dutch roll. Spiral is a divergent motion in bank angle, ψ, and heading angle, ϕ, which is due to a lack of lateral stability and too much directional

stability. A spiral mode is relatively easily to control when identified because it occurs gradually, but if uncorrected, could lead to a spiral divergence. A dihedral wing or increased yaw damping are common methods of mitigating spiral. The Sensorcraft wings have dihedral and therefore the effects of this mode will be more stable. Dutch Roll is an oscillatory mode characterized by the coupling of rolling and yawing motions of the same frequency, but out of phase. There is much controversy over stable spiral and dutch roll properties because designers have found that by improving the stability of one, it can cause a decrease in the stability of the other.

IV. Results

4.1 Initial Complications

The method used to model the velocity values of the wingtip vortices was done with large valued velocities. During the static deflection solution, the receiver wing would deflect through the vortex core of the KC-135 flowfield. The velocity profile of this core is seen in Figure 3.12. The resulting lift on the wing fluctuated significantly at each iteration step as seen in Figure 4.1 (a) and (b). A wing deflecting into the vortex core caused numerical problems when reaching a trimmed solution. This made much of the initial results inconclusive and a trimmed configuration was not reached. To initially ensure that the flowfield velocities were integrated properly within the code, the aircraft was placed in the center of the flowfield (This seemed a logical choice as a place to begin, but the wings flexed into this modeled singularity in the flowfield, causing the wing to experience these extreme fluctuating velocities, preventing the static solution from converging.) This is apparent in Figure 4.1 which shows the lift distribution fluctuation due to the extreme vortex velocities. Portion (a) and (b) show the consecutive iteration once the wing encounters the vortex. The lift distribution lines change from positive (above) and negative (below) the wing. In order to avoid this computational difficulty, the wings were not allowed to flex into the center of the vortex, they could remain infinitely close, but not inside. This was done by placing initial position of the sensorcraft far enough outside of the voretx such that in trimmed configuration the wings did not deflect into the center of the vortex. This did not skew the results of this study due to the fact that the wings could still be close enough to the vortex to experience strong velocities.

4.2 Trimmed Solutions

Table 4.1 is a summary of the achieved trimmed conditions for the flexible and rigid simulations at the orientations specified in the test matrix (Table 3.10). An angle of attack, α, and elevator angle, δ_e, were determined to keep the aircraft in trimmed flight. Note that this study only takes into consideration the elevator

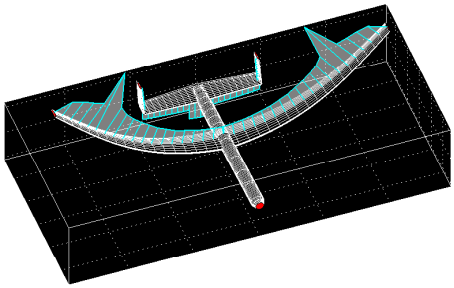

(a) Positive Lift

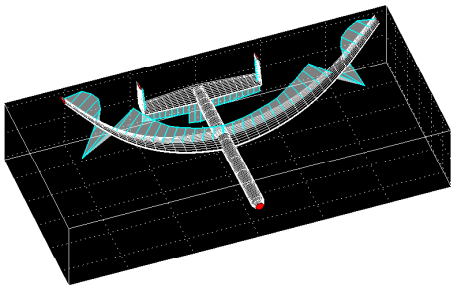

(b) Negative Lift

Figure 4.1: Aircraft with Vortex effects

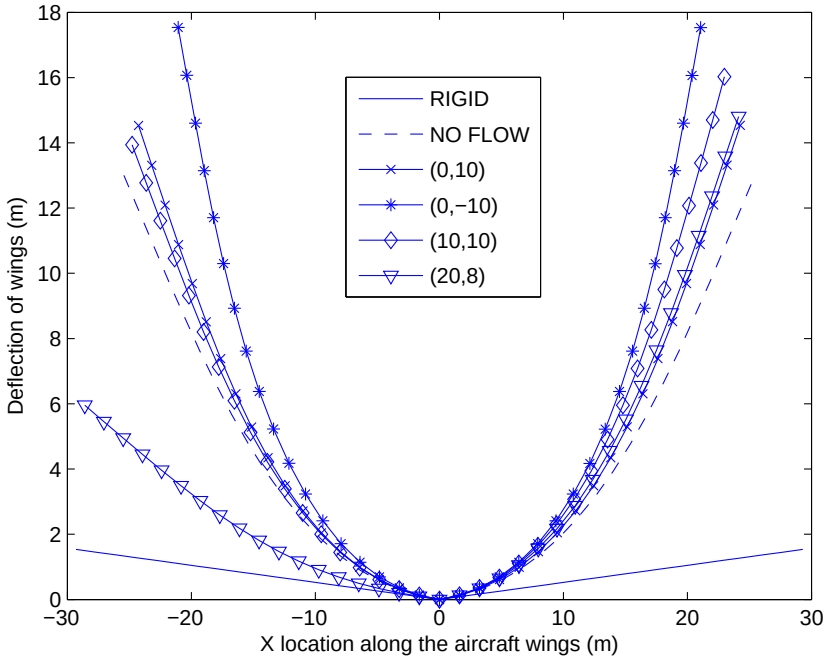

Figure 4.2: Wing Deflection

necessary to keep the aircraft in a trimmed condition, since the flexible nature of the wings creates complexity with aileron control. In addition, Figure 4.2 shows the deflection of the wing for several flowfield locations. Note that the wings are not symmetrically deflected about the origin, specifically for the cases that are off the centerline of the flowfield. This is validation then that the Sensorcraft will experience asymmetric deflection due to the varying flowfield velocities.

4.3 State Space A Matrices and Eigenvalues

Linearizing the EOM's about the trimmed α and δ_e parameters from Table 4.1, the state space A matrices were computed for each of the locations in the flowfield for both the rigid and flexible wing cases. For the rigid cases, there are nine states of interest: three linear velocities, three angular velocities, and three Euler orientation angles. For the flexible cases, there are an additional 144 states which will be explained in more detail in the next section. Note that there are more repre-

sented states for the flexible cases due to the more complex EOM's with elastic states modeled. The eigenvalues of these matrices are used to evaluate the stability of the aircraft. The location of the eigenvalue in the complex plane is indicative of the stability of the aircraft. The eigenvectors of the system reveal which states specifically are contributing to the motion of the aircraft that would make it stable or unstable when perturbed. Both eigenvalues and eigenvectors are presented in the following sections and key findings of each case will be discussed. Classification of aircraft modes of motion will be identified and eigenvalue migration with varying flowfield location will be discussed for the rigid body cases. For the flexible cases, analysis will be slightly different due to the addition of the elastic states, and due to the fact that modes of motion are not traditionally classified for flexible aircraft. That stated, the number and magnitude of unstable eigenvalues and the significant contributions to states denoted by the eigenvectors will be presented.

4.3.1 Rigid Body Cases. The eigenvalues for the rigid body were grouped according to similar values. There are a total of 9 eigenvalues for the rigid body states, six of which are complex pairs with negative real components,one is negative real valued, and an additional two that vary from complex valued to positive real valued. All of the eigenvalues can be seen in Figure 4.3, as well as the relative groupings of the eigenvalues. This figure is used as a means of finding general trends and migrations of the eigenvalues in the complex plane for varying flowfield locations. The different graphical symbols as seen in 4.4 represent the varying locations in the flowfield. The overall view of eigenvalues in the complex plane shows small migrations of the eigenvalues as the aircraft was placed in varying locations. Some of the eigenvalues showed migrations that are worth noting, even though they were minimal and will be explained in the following sections which classify groups of eigenvalues.

4.3.1.1 Dominant Real Negative Eigenvalue. The dominant real eigenvalue of the system as seen at the far left of Figure 4.3 and more distinctly in Figure 4.5, shows the migration of the eigenvalue at varying flowfield location. All of these

Table 4.1: Trimmed Flight Configurations

Location	Rigid α	Rigid δ_e	Flexible α	Flexible δ_e
(0,10) (No Flowfield)	1.76	-8.17	.138	4.17
(0,10)	3.48	-6.95	3.38	1.18
(20,5)	1.07	4.77	1.07	.6396
(-20,5)	1.07	4.77	1.07	.6396
(20,11)	.928	5.37	.9195	1.24
(-20,11)	.928	5.37	.9195	1.24
(0,-10)	2.16	-8.04	1.11	5.95
(0,-30)	2.15	-8.03	.62	3.51
(0,30)	2.39	-7.59	1.09	3.49
(10,-5)	2.62	-7.48	1.48	2.61
(10,10)	1.83	9.72	2.98	2.94

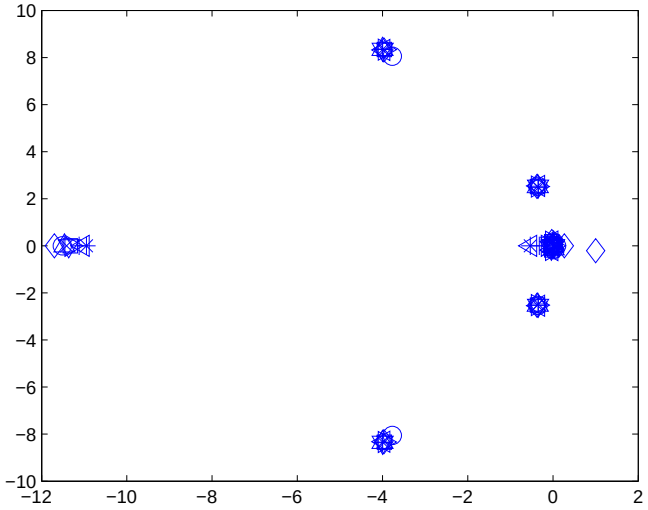

Figure 4.3: Rigid Body Cases: Eigenvalues in Complex Plane

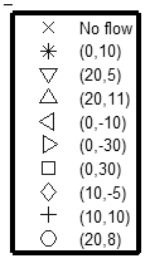

Figure 4.4: Legend of Location Symbols

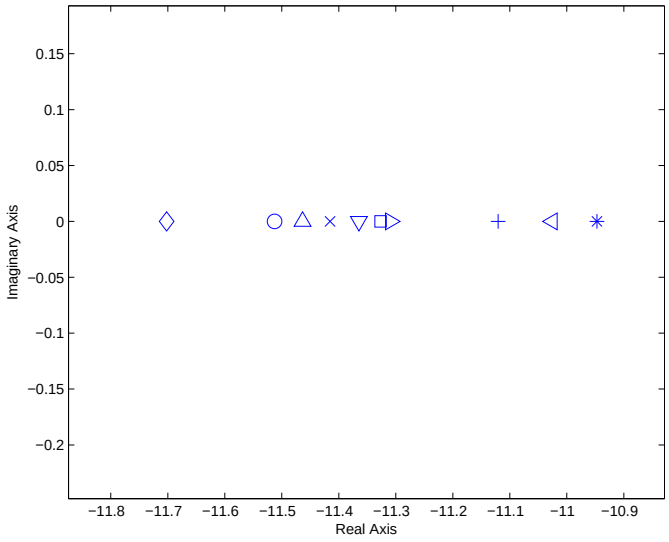

Figure 4.5: Large Scale View of Dominant Real Eigenvalues

eigenvalues are negative and therefore considered stable. It is interesting to note, however, the no flow case denoted by the 'x' was not the farthest left. Indicating that the addition of the flowfield increased the stability for some locations. State contributions for dominant real negative eigenvalues are presented in Tables 4.2 and 4.3. Sensorcraft motion due to the contributions can be considered a stable dutch roll or spiral mode, due to the large contribution of the lateral velocity, which, by the Sensorcraft coordinate system (Figure 3.2), is v_x, and also the contribution to roll rate, as denoted by w_y. The contributions to components of aircraft motion are seen to change as orientation changes within the flowfield. Particular attention can be drawn to the shift in contribution for the $(20, 8)$ case. The v_x component decreases where the w_y component increases.

4.3.1.2 Dominant Complex Eigenvalue Pair. The dominant complex eigenvalue pair is seen in both Figure 4.3 and 4.6. Note that 4.6 shows a close up view of the positive complex value of the eigenvalue pair to show migration. There is very little migration with flowfield location for this eigenvalue pair. The one outlier is the for the $(20, 8)$ case which shows a significant migration from the rest of the eigenvalues

Table 4.2: Dominant Real Negative Eigenvalue: Centerline

Location	No Flow	$(0, 10)$	$(0, -10)$	$(0, -30)$	$(0, 30)$
Eigenvalue	-11.41	-10.94	-11.02	-11.31	-11.32
v_x	0.73	0.69	-0.78	-0.76	0.78
v_y	0	0	0	0	0
v_z	0	0	0	0	0
ω_x	0	0	0	0	0
ω_y	-0.681	-0.71	0.62	0.64	-0.61
ω_z	0.02	-0.02	0.02	0.02	-0.01
ψ	0.0018	-0.002	0.001	0.002	-0.002
ϕ	0.06	0.066	-0.05	-0.05	0.05

Table 4.3: Dominant Real Negative Eigenvalue: Offset

Location	No Flow	$(10, -5)$	$(10, 10)$	$(20, 5)$	$(20, 11)$	$(20, 8)$
Eigenvalue	-11.41	-11.7	-11.12	-11.36	-11.46	-11.51
v_x	0.73	-0.79	0.73	-0.645	-0.62	-0.59
v_y	0	0.006	0.006	0.006	-0.005	0.038
v_z	0	0.07	0.17	0.211	-0.22	0.022
ω_x	0	0.006	0.01	0.016	-0.02	-0.0019
ω_y	-0.681	0.61	-0.65	0.73	0.75	0.8043
ω_z	0.02	0.02	-0.02	0.023	0.02	0.0253
ψ	0.0018	0.002	-0.002	0.002	0.002	0.0022
ϕ	0.06	-0.05	0.05	-0.065	-0.07	-0.0698

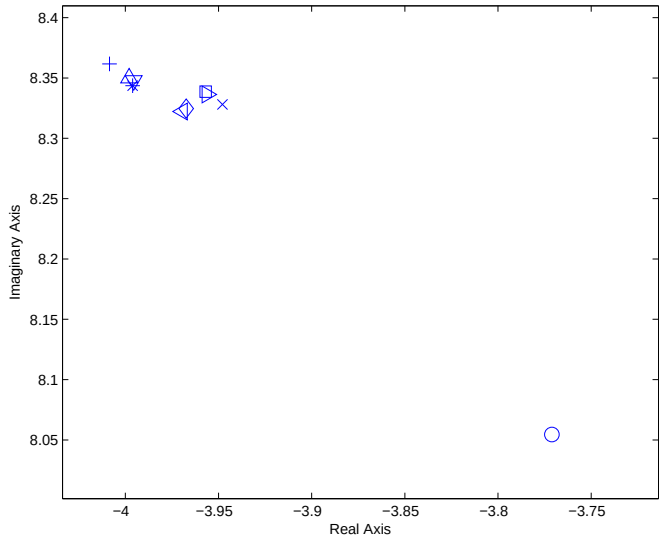

Figure 4.6: Large Scale View of Dominant Complex Eigenvalues

which is due to the strong flowfield velocities near the vortex. State contributions for dominant complex eigenvalues are presented in Tables 4.4 and 4.5. Sensorcraft motion due to the contributions can be considered a longitudinal short period mode due to the strong contribution of the vertical velocity, denoted by v_z. The pitch rate also has a contribution which remains essentially constant for all locations within the flowfield. This is representative of short period mode which is characterized by changes in pitch attitude and angle of attack. It also must be noted that there is a contribution of the v_y component which is considered a lateral component. Due to the minimal contribution of the ω_y, ω_z, ψ, and ϕ components, they were omitted from the table.

Table 4.4: Dominant Complex Eigenvalue: Centerline

Location	No Flow	$(0, 10)$	$(0, -10)$	$(0, -30)$	$(0, 30)$
Eigenvalue	-3.94(+/-)8.32i	-3.99(+/-)8.34i	-3.96(+/-)8.32i	-3.95(+/-)8.33i	-3.95(+/-)8.33i
v_x	0	0	0	0	0
v_y	0.0184-0.0352i	0.0101-0.0317i	0.0248-0.0379i	0.0243-0.0377i	0.0286-0.0395i
v_z	0.9981	0.9983	0.9979	0.9979	0.9977
ω_x	0.0022-0.0465i	0.0024-0.0466i	0.0023-0.0464i	0.0022-0.0465i	0.002-0.0465i
θ	-0.0047+0.0019i	-0.0047+0.0019i	-0.0047+0.0019i	-0.0047+0.0019i	-0.0047+0.0019i

4.3.1.3 Intermediate Complex Eigenvalue Pair. The intermediate eigenvalue pair can be seen in 4.3 located near the origin. The term intermediate in this case is used as means to classify the eigenvalue pair that has a real component in between the least valued and dominant valued pair. Figure 4.7 shows a close up view of the positive complex value of the eigenvalue pair to show migration. There is very minimal migration for this pair and noting significant to note. State contribution for the intermediate valued eigenvalue pair are presented in Table 4.6 and 4.7. Sensorcraft Motion due to the contributions can be classified as a lateral mode of motion. Whether this mode is considered a dutch roll or spiral is difficult to classify. As presented in Tables there is a strong contribution of the lateral velocity, which is denoted as v_x, and small contributions of the w_y, w_z, ψ and ϕ components. The pitch rate, w_x, and pitch angle, θ, components were considered insignificant and omitted from the table. Of particular importance is the flowfield at location $(20, 8)$. A considerable two order of magnitude increase in the contribution of the v_z component occurs. Being a longitudinal component, further nonlinear stability analysis would need to be done to determine stability for this orientation.

4.3.1.4 Least Valued Complex Eigenvalue Pair. The least valued complex eigenvalue pair is shown in Figure 4.3 clustered around the origin of the complex plane and a more close up view is shown in Figure 4.8 is of the positive complex value of the eigenvalue pair to show migration. There is very little migration of these eigenvalues, however since they are very close to the positive real axis, a small migration could lead to instability. State contribution for the eigenvalues with the least real portion are presented in Tables 4.8 and 4.9. Senorcraft motion due to these contributions

Table 4.5: Dominant Complex Eigenvalue: Offset

Location	No Flow	$(10, -5)$	$(10, 10)$	$(20, 5)$	$(20, 11)$	$(20, 8)$
Eigenvalue	-3.94(+/-)8.32i	-3.96(+/-)8.32i	-4(+/-)8.36i	-3.99(+/-)8.34i	-3.99(+/-)8.35i	-3.77(+/-)8.05i
v_x	0	-0.0018-0.0013i	0.0015+0.0012i	-0.0020-0.0016i	-0.0016-0.0012i	0.0011+0.0020i
v_y	0.0184-0.035i	-0.0328+0.041i	0.0204-0.035i	-0.0077+0.03i	-0.0055+0.03i	-0.0019-0.0335i
v_z	0.9981	-0.9975	0.998	-0.9984	-0.9984	0.9984
ω_x	0.0022-0.046i	-0.0023+0.046i	0.0025-0.046i	-0.0024+0.046i	-0.0025+0.046i	0.0021-0.0448i
θ	-0.0047+0.001i	0.0047-0.002i	-0.0047+0.002i	0.0047-0.002i	0.0047-0.002i	-0.0047+0.0019i

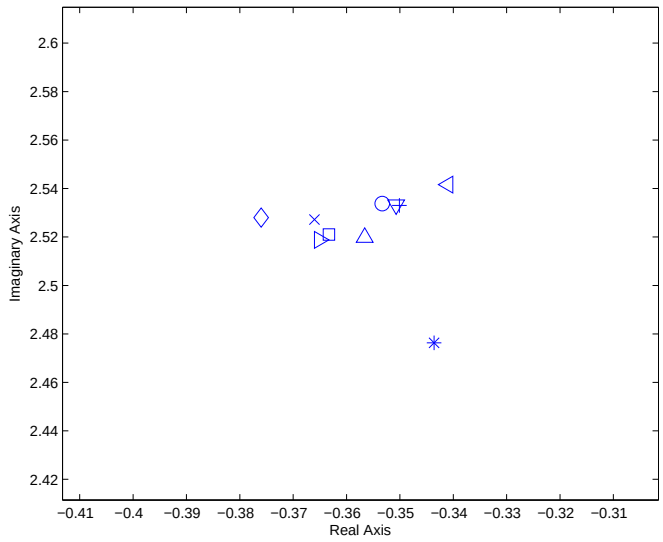

Figure 4.7: Large Scale View of Intermediate Complex Eigenvalues

10pt

Table 4.6: Intermediate Complex Eigenvalue: Centerline

Location	No Flow	$(0, 10)$	$(0, -10)$	$(0, -30)$	$(0, 30)$
Eigenvalue	-.37 (+/ -) 2.52i	-.34 (+/ -) 2.47i	-.34 (+/ -) 2.54i	-.37 (+/ -) 2.51i	-.36 (+/ -) 2.52i
v_x	0.9999	0.9999	-0.9999	0.9999	-0.9999
v_y	0	0.0000 + 0.0000i	-0.0000 + 0.0000i	0.0000 + 0.0000i	0.0000 + 0.0000i
v_z	0	-0.0000 + 0.0000i	0.0000 - 0.0000i	0.0000 - 0.0000i	-0.0000 + 0.0000i
ω_y	-0.0037 - 0.0010i	-0.0039 - 0.0016i	0.0039 + 0.0019i	-0.0039 - 0.0011i	0.0039 + 0.0012i
ω_z	-0.0005 + 0.0128i	-0.0004 + 0.0125i	0.0003 - 0.0129i	-0.0005 + 0.0128i	0.0004 - 0.0128i
ψ	-0.0050 + 0.0005i	-0.0050 + 0.0005i	0.0050 - 0.0005i	-0.0050 + 0.0005i	0.0050 - 0.0005i
ϕ	-0.0003 + 0.0015i	-0.0005 + 0.0016i	0.0007 - 0.0016i	-0.0004 + 0.0016i	0.0004 - 0.0016i

Table 4.7: Intermediate Complex Eigenvalue: OffSet

Location	No Flow	$(10, -5)$	$(10, 10)$	$(20, 5)$	$(20, 11)$	$(20, 8)$
Eigenvalue	-.37(+/-) 2.52i	-.37(+/ -)2.52i	-.35(+/-)2.53i	-.35(+/-)2.53i	-.36(+/-) 2.52i	-.35(+/-)2.53i
v_x	0.9999	-0.9999	0.9998	0.9999	-0.9998	0.9997
v_y	0	0.0007	0.0006	-0.0009	-0.0008	0.0046 + 0.0023i
v_z	0	-0.0021+0.004i	-0.0004+0.012i	0.0006-0.0081i	0.0001-0.0157i	-0.0137+0.0111i
ω_y	-0.0037-0.0010i	0.0036+0.0007i	-0.0039-0.0014i	-0.0036-0.0007i	0.0036+0.0006i	-0.0036
ω_z	-0.0005+0.0128i	0.0005-0.013i	-0.0004+0.013i	-0.0005+0.013i	0.0005-0.0127i	-0.0005+0.0128i
ψ	-0.0050+0.0005i	0.0050-0.0005i	-0.0050	-0.0050	0.0050-0.0005i	-0.0050
ϕ	-0.0003+0.002i	0.0003-0.002i	-0.0005+0.002i	-0.0002+0.002i	0.0001-0.0015i	-0.0000+0.001i

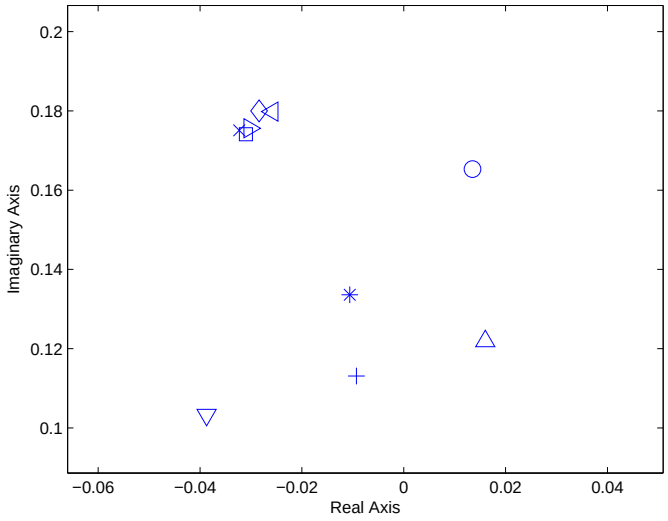

Figure 4.8: Large Scale View of Dominant Real Eigenvalues

can be classified as a longitudinal phugoid mode. A there is a strong contribution to the longitudinal velocity, denoted as v_y in the table and also a significant contribution to the vertical velocity, as denoted by v_z. This is representative of the phugoid mode characterized by significant changes in forward speed. The values of the v_z component vary with the location within the flowfield which will be an indicator of stability based on damping and frequency of the mode. The yaw rate, w_z, component was omitted due to insignificant contributions.

4.3.1.5 Additional Eigenvalues. The additional eigenvalues are shown in Figure 4.3 and 4.9 in a more close up view. It is more difficult to classify these because some have slightly complex portions, but in general, migrations from the

Table 4.8: Least Valued Complex Eigenvalue Pair: Centerline

Location	No Flow	$(0, 10)$	$(0, -10)$	$(0, -30)$	$(0, 30)$
Eigenvalue	-.032 (+/ -) .18i	-.011 (+/ -) .14i	-.026 (+/ -) .18i	-.03 (+/ -) .18i	-.031 (+/ -) .17i
v_x	0	0.0001 + 0.0000i	0.0000 - 0.0000i	0.0000 - 0.0000i	0.0000 - 0.0000i
v_y	-0.9935	-0.9989	0.9905	-0.9929	-0.9939
v_z	0.1122 - 0.0019i	0.0448 - 0.0061i	-0.1340 + 0.0252i	0.1178 - 0.0025i	0.1091 - 0.0021i
ω_x	-0.0032 - 0.0000i	-0.0018 + 0.0002i	0.0032 - 0.0003i	-0.0032 + 0.0001i	-0.0031 + 0.0001i
ω_y	0	0.0000 + 0.0000i	-0.0000 - 0.0000i	0.0000 + 0.0000i	0.0000 + 0.0000i
ψ	0	-0.0000 - 0.0000i	0.0000 + 0.0000i	-0.0000 - 0.0000i	-0.0000 - 0.0000i
θ	0.0030 + 0.0177i	0.0022 + 0.0133i	-0.0042 - 0.0174i	0.0036 + 0.0175i	0.0037 + 0.0173i
ϕ	0	0.0000 - 0.0000i	-0.0000 + 0.0000i	0.0000 - 0.0000i	0.0000 - 0.0000i

left half plane to the right half plane are seen in this grouping. The most severe case was the $(10, -5)$ case which was most likely due to the asymetric loading on the wings at this location off centerline and below the vortices. The flowfield at this location can be seen in Figure 3.14. State contributions for the remaining eigenvalues are presented in Tables 4.10 and 4.11. The eigenvalues vary to include complex and real values both positive and negative. Analysis of these remaining eigenvalues will be accomplished differently since modes of motion cannot be identified. For the case with no flow, it can be seen that the eigenvalues are considered to be marginally stable the largest contributions to motion in the Euler Yaw Angle, ψ. Adding the flowfield, shows the strong contribution to the lateral velocity,v_x, components. Movement in the flowfield off the centerline, in general places the eigenvalues in the right half plane. There is little correlation, however, between the dominant contributions when moving throughout the flowfield. Referencing Table 4.11 for the cases off the centerline, the $(10, -5)$ case shows varying contributions of motion with strong contributions from v_x, v_y, and v_z components as well as contributions from ψ and ϕ. Lateral and Longitudinal modes would influence the stability of the aircraft at this orientation.

4.3.2 Flexible Cases. Analysis of the flexible cases for stability was modified from the rigid body cases because of the number of states involved. There are 153 total states for the elastic cases, the first 144 states consist of elastic strains, ϵ, and strain rates $\dot{\epsilon}$. Figure 4.11 illustrates more clearly the numbering of the states, which is necessary to interpret the results. The strain and strain rates are divided into extension strain, twist strain, out-of-plane bending strain, and in-plane bending strain

Table 4.9: Least Valued Complex Eigenvalue Pair: Offset

Location	$(0, 10)$no flow	$(10, -5)$	$(10, 10)$	$(20, 5)$	$(20, 11)$	$(20, 8)$
Eigenvalue	-.032(+/-).18i	-.032(+/-).18i	-.01(+/-).11i	-.039(+/-).11i	-.016(+/-).12i	-.014 (+/-) .17i
v_x	0	-0.0073+0.012i	-0.0078-0.001i	0.0347-0.085i	0.0170+0.035i	0.0420+0.0304i
v_y	-0.9935	0.9906	-0.9998	-0.9871	0.9931	0.9973
v_z	0.1122-0.002i	-0.1345+0.01i	0.0083-0.0013i	-0.0498+0.112i	0.0145+0.108i	0.0193 + 0.0448i
ω_x	-0.0032	0.0033	-0.0013	-0.0011	0.0013	0.0015
ω_y	0	-0.0010	0.0000	0.0015+0.0014i	-0.0017	-0.0017
ψ	0	0.0014	-0.0003-0.002i	-0.0082	0.0057	0.0033-0.001i
θ	0.0030+0.0177i	-0.0046-0.018i	0.0018+0.011i	-0.0018+0.012i	-0.0038-0.011i	0.0007 - 0.0090i
ϕ	0	0.0033 + 0.005i	0.0055	0.0074-0.0171i	0.0011+0.0140i	0.0042+0.0109i

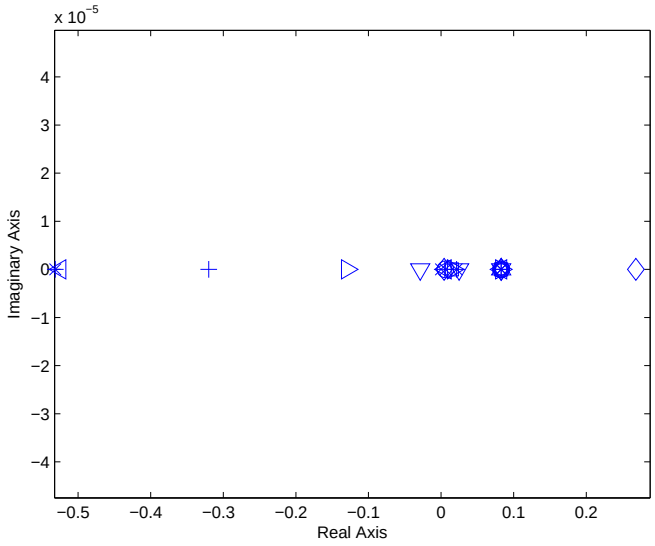

Figure 4.9: Large Scale View of Additional Eigenvalues

Table 4.10: Additional Eigenvalues: Centerline

Location	No Flow	No Flow	$(0, 10)$	$(0, 10)$	$(0, -10)$	$(0, -10)$	$(0, -30)$	$(0, -30)$	$(0, 30)$	$(0, 30)$
Eigenvalue	0	0.0061	-0.53	0.0214	-0.5244	0.0063	0.0164	-0.1296	0.0149	-0.1225
v_x	0	0.083	-0.9956	-0.9914	0.9967	-0.8743	0.6022	-0.9519	-0.0901	-0.9778
v_y	0	0	0	0.0014	-0.0001	-0.0001	0.0026	-0.0012	0.0205	-0.0015
v_z	0	0	-0.0004	0.0002	0.0003	0	0.0001	-0.0001	0.001	-0.0002
ω_x	0	0	0	0	0	0	0	0	0	0
ω_y	0	0.0006	0.0435	0.0004	-0.0377	-0.0003	-0.0035	0.0374	-0.0038	0.0242
ω_z	0	-0.006	0.0057	-0.0028	-0.0047	0.003	0.0124	0.0135	0.0141	0.0088
ψ	1	0.9891	0.0107	0.129	-0.0091	-0.4812	-0.7602	0.1046	-0.9513	0.0723
θ	0	0	0	0	0	0.0001	-0.0001	0	-0.0002	0
ϕ	0	0.1219	-0.0817	0.0232	0.0715	-0.0641	-0.2437	-0.2851	-0.2937	-0.1949

Table 4.11: Additional Eigenvalues: Offset

Location	$(10, -5)$	$(10, -5)$	$(10, 10)$	$(10, 10)$	$(20, 5)$	$(20, 5)$	$(20, 11)$	$(20, 8)$	$(20, 8)$
Eigenvalue	0.0041	0.2683	-0.32	0.0051	0.0249	-0.0288	-.0005 (+/ -) .011i	0.0058	0.0827
v_x	-0.2146	0.6627	0.6694	0.0454	-0.1174	0.2713	-0.0820 + 0.2393i	-0.0566	0.2814
v_y	-0.94	-0.4316	0.0592	0.9823	0.9759	-0.8886	0.9418	-0.9502	0.9493
v_z	-0.0339	-0.5759	0.7298	0.0909	0.176	-0.3547	0.1321 + 0.1350i	-0.2794	0.0962
ω_x	0	0.0021	-0.0034	0	-0.0001	0.0001	0.0000 + 0.0000i	-0.0001	0.0034
ω_y	0	0.052	-0.0379	0.0001	-0.0006	-0.0016	-0.0002 + 0.0001i	-0.0001	0.0065
ω_z	-0.0011	-0.0114	-0.0055	-0.0008	0.0012	-0.0026	-0.0009 - 0.0008i	0.0007	-0.004
ψ	0.2623	0.0424	-0.0172	0.1562	-0.0471	-0.0897	0.0704 - 0.0884i	-0.1237	0.0487
θ	0.0004	0.0078	0.0108	-0.0005	-0.0024	-0.0029	0.0000 - 0.0010i	-0.0202	0.0416
ϕ	0.0202	0.1957	0.1179	0.0164	-0.0242	0.0529	0.0148 + 0.0202i	-0.0141	0.0791

at nine locations along the wings. In addition, Table A.4 in the appendix contains all of the numbered states and where they are measured. As stated previously, the analysis for the flexible cases will be completed differently due to the shear volume of information. In an effort to illustrate the complexity of stability analysis for a flexible aircraft a similar plot of the eigenvalues in the complex plane is shown in Figure 4.10. There are no significant groupings as was seen for the rigid cases that are easily classifiable. This is due to the fact that the flexible states are continually changing due to the varying velocities in the flowfield. A stable eigenvalue in one location may significantly shift location along the real and imaginary axis. An example of these shifts is also seen by the $(10, 10)$ case denoted as the '+' on the far right of the eigenvalue plot. The magnitude of the eigenvalue migrated considerably from the rest. Stability analysis for the flexible cases was only completed for the most crucial flowfield cases which were determined to be a baseline with no flowfield, $(0, 10)$, $(0, -10)$, $(10, 10)$ and $(20, 8)$. From these cases, the dominant positive eigenvalues were chosen, then contributions from each state were examined. Dominant eigenvalues were relative to the location in the flowfield, and will be discussed in each section. All cases were shown to have positive eigenvalues which is an indicator of instability, but the most severe cases will be addressed.

4.3.2.1 No KC-135 Flowfield. The no KC-135 flowfield cases had two dominant positive eigenvalues each with significant contributions from many states. The Tables 4.12 and 4.13 show the dominant eigenvalues and corresponding dominant state contributions. Dominant eigenvalues were considered to be with a real portion greater than zero. These tables show the states that exhibited a more than 0.1 eigenvector magnitude which was considered to be a significant contribution. There are significant contributions to the in-plane and extension strain rates from elements for both members. The eigenvalue as shown in Table 4.13 has strong contributions in v_y, ψ, and ϕ. The fact that the Sensorcraft is unstable without the influence of the flowfield in this case is a significant area which will need to be addressed later on.

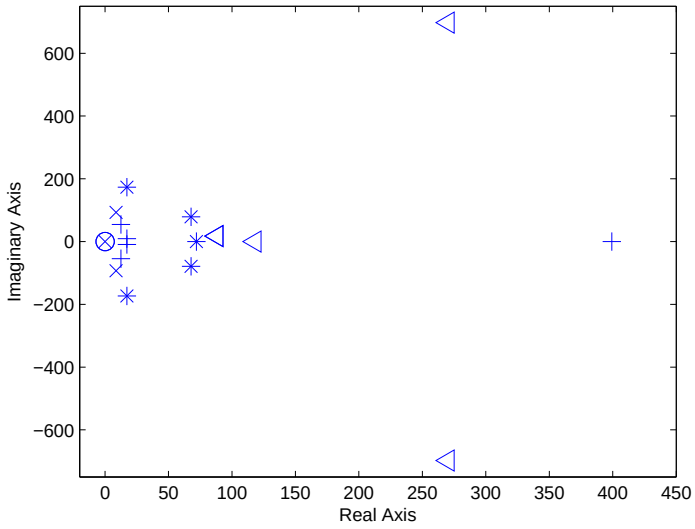

Figure 4.10: Flexible Cases: Eigenvalues in Complex Plane

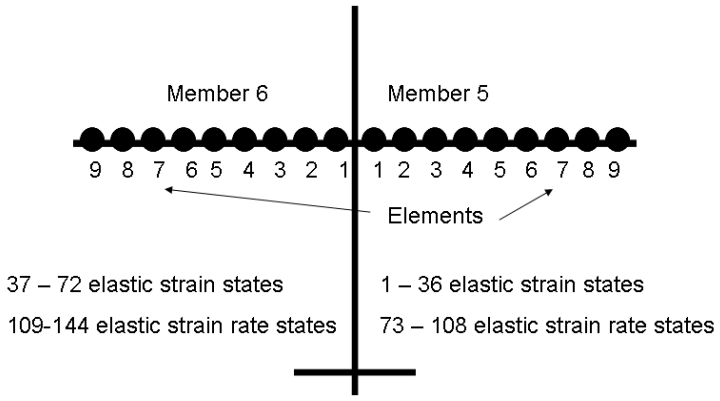

Figure 4.11: Elastic States

Table 4.12: No Flowfield- Eigenvalue Pair: 8.6599 (+/-) 93.069i

State Number	Contribution
82	0.12528
86	0.22617
87	0.10311
90	0.26639
91	0.10036
94	0.33656
95	0.16529
98	0.40629
99	0.26913
102	0.39148
103	0.44934
106	0.17094
107	0.23467

Table 4.13: No Flowfield- Eigenvalue: .0359

State Number	Contribution
146	0.58286
151	0.61994
153	0.43768

4.3.3 Location $(0, 10)$. Adding the KC-135 flowfield to the simulation at location $(0, 10)$ there were more eigenvalues that moved into the right half plane, which indicates a change in stability. Dominant eigenvalues were considered to be with a real portion greater than 5. The first eigenvalue pair as shown in Table 4.14, shows significant contributions to the extension and twist strain rates. Note that these contributions are located on the outermost location of the wings, which by the nature of the Sensorcraft design will be changing position within the flowfield. Therefore, it is appropriate that there are the most contributions to the states at these locations. It is interesting to note that dominant states affected were not symmetrical between member 5 and 6 even though the location in the flowfield was not yet moved off the centerline of the flowfield. This asymmetry was also noted in the rigid body cases where deflection at steady state was different for the each wing (Figure 4.2).

4.3.4 Location $(0, -10)$. Moving the orientation of the aircraft again in the KC-135 flowfield, now to beneath the vortices, there are the most significant eigenvalues. Dominant eigenvalues were considered to be those with a real portion of greater than 30 because there were so many to consider. Eigenvalues in Tables 4.17, 4.18, 4.19, and 4.20 show significant contributions in twist,extension rate, out-of-plane strain rate mostly at the outermost elements on the wings.

4.3.5 Location $(10, 10)$. Moving the orientation off the centerline of the KC-135 flowfield, the eigenvalues make a significant shift into the right half plane. The dominant eigenvalue for this location are considered to be greater than 5. The eigenvalues and state contributions for this case are shown in Tables 4.21,4.22, and 4.23. The presence of unstable eigenvalues in this case is due to the asymmetric flowfield parameters when moving off the centerline. Eigenvalues at this orientation show strong contribution to twist strain rate, extension strain rate, in-plane, and out of plane mostly along the the elements in member 6, which is considered the left wing. This occurred because the Sensorcraft is off centerline of the flowfield, so the right

Table 4.14: Location $(0, 10)$ - Eigenvalue Pair: 17.253 (+/-) 173.54i

State Number	Contribution
115	0.15905
119	0.18898
123	0.17914
126	0.15193
127	0.3386
130	0.20459
131	0.39874
134	0.17312
135	0.32844
138	0.12136
139	0.51146
143	0.34783

Table 4.15: Location $(0, 10)$ - Eigenvalue Pair: 67.78 (+/-) 78.964i

State Number	Contribution
91	0.2727
95	0.17232
99	0.44525
103	0.72999
107	0.37173

Table 4.16: Location $(0, 10)$ - Eigenvalue: 72.077

State Number	Contribution
126	0.18989
127	0.27502
130	0.37263
131	0.38663
134	0.46088
135	0.36876
138	0.41907
139	0.20262
142	0.12905

Table 4.17: Location $(0, -10)$ - Eigenvalue Pair: 270.22 (+/-) 697.6i

State Number	Contribution
127	0.79058
130	0.18306
131	0.11624
134	0.21847
138	0.15002
139	0.13719
142	0.28276
143	0.38034

Table 4.18: Location $(0, -10)$ - Eigenvalue Pair: 57.415 (+/-) 299037i

State Number	Contribution
91	0.36678
94	0.21552
95	0.23012
98	0.26123
99	0.44971
102	0.28797
103	0.18602
106	0.27543
107	0.54188

Table 4.19: Location $(0, -10)$ - Eigenvalue Pair: 88.174 (+/-) 17.675i

State Number	Contribution
90	0.14445
91	0.22204
94	0.32475
95	0.29326
98	0.42475
99	0.37313
102	0.40501
103	0.40396
106	0.12639
107	0.25374

wing (member 5) is not as affected by the downward velocities of the vortex beneath the KC-135.

4.3.6 Location $(20, 8)$. The results for this orientation were an abberation to previous results. Dominant eigenvalues in this case were only slightly in the right half plane, so dominant eigenvalues were considered anything positive. The first eigenvalue as shown in Table 4.24 shows significant contribution to most of rigid body states, v_x, v_y, v_z, $\dot{\psi}$, $\dot{\theta}$, and $\dot{\phi}$. The largest contributor being the v_y component. The second and final eigenvalue, as shown in Table 4.25, shows significant contribution in v_x, v_y, v_z, and ψ. It is interesting that the case located closest to the most intense velocities of the flowfield actually ended up being the most stable flexible case. This due to the fact that the most intense velocities are nearest the fuselage of the Sensorcraft. The deflection of the wing nearest the fuselage will less for an intense flowfield velocity than it will be at the wingtips where an intense flowfield velocity will cause severe deflection of the wings, and, in turn, more unfavorable force and moment contributions that will lead to instability.

Table 4.20: Location $(0, -10)$ - Eigenvalue: 118.11

State Number	Contribution
87	0.11681
90	0.14581
91	0.31009
94	0.36845
95	0.26333
98	0.47034
99	0.20913
102	0.4343
103	0.32429
106	0.11471
107	0.29796

Table 4.21: Location $(10, 10)$ - Eigenvalue: 399.27

State Number	Contribution
123	0.11459
127	0.66598
130	0.3039
134	0.33914
138	0.29541
139	0.22432
143	0.41567

Table 4.22: Location $(10, 10)$ - Eigenvalue Pair: 12.588 (+/-) 54.43i

State Number	Contribution
87	0.16055
94	0.12733
98	0.13145
99	0.15628
102	0.10214
103	0.21313
119	0.10884
122	0.12836
123	0.10546
126	0.21807
130	0.32016
131	0.18332
134	0.37699
135	0.3153
138	0.33836
139	0.31989
142	0.12358
143	0.17744
149	0.15145

Table 4.23: Location $(10, 10)$ - Eigenvalue Pair: 17.214 (+/-) 9.1836i

State Number	Contribution
86	0.11072
87	0.26048
90	0.1785
91	0.40774
94	0.24795
95	0.44998
98	0.27778
99	0.39541
102	0.23857
103	0.30285
107	0.12416
147	0.14512

Table 4.24: Location $(20, 8)$ - Eigenvalue: .1016

State Number	Contribution
145	0.31754
146	0.88952
147	0.17553
151	0.10143
152	0.1196
153	0.2272

Table 4.25: Location $(20, 8)$ - Eigenvalue: .0131

State Number	Contribution
145	0.25906
146	0.5692
147	0.7168
151	0.2928

V. Conclusions and Recommendations

5.1 Conclusions

The conclusions of this research reveal many of issues that will need to be addressed in order to accomplish a successful refueling mission of a flexible winged aircraft. The findings presented in this research, however, have narrowed some of the key areas which will need attention when designing a controller. Areas of the flowfield that will cause the aircraft to have assymetric loading on the wings, meaning locations that are not centered in the flowfield will be the most apt to experience instabilities. Although the typical refueling approach of a receiver aircraft is from behind and below, and ideally would be centered behind the refueling aircraft, the flexibility of the wings, controllability of the Sensorcraft, the possibility of adverse wind conditions, and a multitude of other factors will not guarantee the optimal approach. That stated, of the cases presented in this research, both for rigid and flexible wings, the magnitude of instability between cases in which the receiver is placed in the center of the flowfield versus off center at a variety of locations is significantly different. The most severe case of instability were found for the off centerline cases in the elastic states when placed 10 meters off centerline. The $(20, 8)$ case was an abberation with only two unstable eigenvalues only merely in the right half plane, the forces and moments centered near the fuselage.

5.2 Recommendations for Future Research

Since this research draws from a variety of sources, it is important to address all areas in which future research will benefit. The majority of this research deals with the initial setup of the refueling situation and integrating the models so there were many limitations for these initial computations that can be analyzed in a more thorough analysis.

5.2.1 Recommendations for the Flowfield Data. The computational issues which evolved from the aircraft encountering the velocities in the vortex of the flow-

field did not allow the aircraft to be simulated where the aircraft wings would be in the center of the vortex. The wings could be close, but once the wing deflected to the center of the vortex it was unable to reach a numerical solution due to the computational method used. For these sections of the flowfield, it would be beneficial to develop a method that could handle large fluctuations in forces on the wings and still arrive at a trimmed solution, or perhaps a different method of flowfield data integration would need to be developed to capture these areas. Because of the inherent difficulty of controlling a flexible winged aircraft, to ensure it would remain outside of these areas would be too stringent of an assumption. For the cases run, the refueling aircraft was assumed to be at it's heaviest configuration because the flowfield velocities would be more extreme. Flowfield data for different weight configurations was tabulated and therefore a lightweight condition could also be explored to see if there are great differences in stability due to the change in flowfield velocities with a lighter refueling aircraft.

Most of the conclusions of this research do not present a definitive answer in a stability sense. There are certain states to have been found unstable for the flexible and rigid cases, but the actual implications on the overall stability are not exactly known. This research allowed for the development of a method and the tools in order to find the areas on the aircraft that are more unstable than others. Knowing these areas will be beneficial in developing a controller for the aircraft. Identification of unstable states must be done before a control design can be implemented and the controllability of the state is determined. Many of the flexible states are not traditional, so in order to try and control states that are not normally realized in aircraft motion will be another challenge. An example of this would be using a sort of spoiler to minimize in-plane strain rates. This research can be used as a tool for a relative determination of stability of the aircraft and has many areas which can be improved to create a more precise determination. These areas will be addressed in the following section.

5.3 Recommendations for Trimming Solution

The Sensorcraft model in this research was trimmed solely using the elevator control surface, but there is the ability to add the aileron and rudder inputs required for trimmed flight. Computationally, this will require much more time as the solution will require many iterations to converge to a trimmed solution. Allowing for thrust to be a search variable for the trimmed solution rather than holding it constant would also be another modification to the trimming routine. Because of the weight transfer that occurs during refueling, it will be crucial to eventually model the changes that arise with the aircraft's inertia properties. At the beginning of the refueling process they will be drastically different than at the end and whether or not they adversely effect or benefit the stability of the aircraft, they cannot be overlooked. Simulating the aircraft at varying altitudes will also help with the stability analysis by providing a best case scenario for both the Sensorcraft and the refueling aircraft. The Sensorcraft typically flies at high altitudes, although this can depend on the specific application, and therefore the complication of maneuvering down to an altitude where the KC-135 can refuel (which normally does not exceed 10.6 km (35000ft)) must be addressed. The variation of airspeed could also be changed to note the effects on stability, but will also have limitations as the KC-135 airspeed will need to remain within the refueling envelope.

5.4 Recommendations for a Controller

Due to the dynamic conditions the aircraft will encounter when flying behind a refueling aircraft, and completion of basic flight maneuvers that this aircraft will need to preform to refuel, control will present many challenges to ensure it's unstable states are controllable. Determination of these uncontrollable states can be done with similar analysis done in this work, but with many more simulations completed. The controller would need to be dependent on the forces encountered at different areas which could possibly be a function of pressures or perhaps a location that is determined once the aircraft is within a region of interest of the refueling aircraft.

5.5 Aircraft Stiffness

For these simulations, the stiffness of the wings was set for a certain tolerance and allowed to deflect to a certain degree. To examine stability, these specifications could be simulated more strictly or relaxed. There is the inherent tradeoff between stiffness and weight which would need to be considered, but the reliability of an appropriate controller could possibly be outweighed by modifying the structural makeup of the aircraft.

5.6 General Remarks

Continued research in all of these areas will benefit the aerial refueling research efforts of many other endeavors beyond this aircraft. A refueling mission is an important aspect for any aircraft to be able to complete because it enables the aircraft to extend its mission duration as well as alleviate complications of returning to a nearby base which may not be possible. As aircraft become more complex, incorporating new concepts and designs that will exhibit varying behaviors there will be the constant need to analyze the feasibility of refueling. The thought of changing the refueling methods already developed would uncover many more possibilities. Changing orientation of the refueling configuration, placing the receiver aircraft in front of the refueling aircraft, would be a possibility, but with the receiver aircraft flowfield effecting the refueling aircraft. Noting that the refueling aircraft's flowfield would also have an effect of "pushing" the lightweight Sensorcraft by the effects of its flowfield. Perhaps an even more drastic recommendation would be to introduce another type of refueling aircraft into the inventory. One that had a larger wingspan than the current KC-135, and also greater than that of HALE/Sensorcraft vehicles with such large aspect ratio wings, could possibly create a more stable environment for the Sensorcraft. Regardless of the location in the flowfield or refueling aircraft used to successfully refuel, this research supports the fact that much analysis of the behavior of a flexible Sensorcraft must be analyzed in order to develop an adequate controller and optimal locations within the flowfield will aid in the overall stability of the aircraft.

Appendix A. States for Flexible Model

Table A.1: States for Flexible Model

State Number	Contribution
1	Member 5 Element 1 Extension Strain
2	Member 5 Element 1 Twist Strain
3	Member 5 Element 1 Out of Plane Strain
4	Member 5 Element 1 In Plane Strain
5	Member 5 Element 2 Extension Strain
6	Member 5 Element 2 Twist Strain
7	Member 5 Element 2 Out of Plane Strain
8	Member 5 Element 2 In Plane Strain
9	Member 5 Element 3 Extension Strain
10	Member 5 Element 3 Twist Strain
11	Member 5 Element 3 Out of Plane Strain
12	Member 5 Element 3 In Plane Strain
13	Member 5 Element 4 Extension Strain
14	Member 5 Element 4 Twist Strain
15	Member 5 Element 4 Out of Plane Strain
16	Member 5 Element 4 In Plane Strain
17	Member 5 Element 5 Extension Strain
18	Member 5 Element 5 Twist Strain
19	Member 5 Element 5 Out of Plane Strain
20	Member 5 Element 5 In Plane Strain
21	Member 5 Element 6 Extension Strain
22	Member 5 Element 6 Twist Strain
23	Member 5 Element 6 Out of Plane Strain
24	Member 5 Element 6 In Plane Strain
25	Member 5 Element 7 Extension Strain
26	Member 5 Element 7 Twist Strain
27	Member 5 Element 7 Out of Plane Strain
28	Member 5 Element 7 In Plane Strain
29	Member 5 Element8 Extension Strain
30	Member 5 Element 8 Twist Strain
31	Member 5 Element 8 Out of Plane Strain
32	Member 5 Element 8 In Plane Strain
33	Member 5 Element 9 Extension Strain
34	Member 5 Element 9 Twist Strain
35	Member 5 Element 9 Out of Plane Strain
36	Member 5 Element 9 In Plane Strain
37	Member 6 Element 1 Extension Strain
38	Member 6 Element 1 Twist Strain
39	Member 6 Element 1 Out of Plane Strain

Table A.2: States for Flexible Model (cont.)

State Number	Contribution
40	Member 6 Element 1 In Plane Strain
41	Member 6 Element 2 Extension Strain
42	Member 6 Element 2 Twist Strain
43	Member 6 Element 2 Out of Plane Strain
44	Member 6 Element 2 In Plane Strain
45	Member 6 Element 3 Extension Strain
46	Member 6 Element 3 Twist Strain
47	Member 6 Element 3 Out of Plane Strain
48	Member 6 Element 3 In Plane Strain
49	Member 6 Element 4 Extension Strain
50	Member 6 Element 4 Twist Strain
51	Member 6 Element 4 Out of Plane Strain
52	Member 6 Element 4 In Plane Strain
53	Member 6 Element 5 Extension Strain
54	Member 6 Element 5 Twist Strain
55	Member 6 Element 5 Out of Plane Strain
56	Member 6 Element 5 In Plane Strain
57	Member 6 Element 6 Extension Strain
58	Member 6 Element 6 Twist Strain
59	Member 6 Element 6 Out of Plane Strain
60	Member 6 Element 6 Extension Strain
61	Member 6 Element 7 Twist Strain
62	Member 6 Element 7 Out of Plane Strain
63	Member 6 Element 7 In Plane Strain
64	Member 6 Element 7 Extension Strain
65	Member 6 Element8 Twist Strain
66	Member 6 Element 8 Out of Plane Strain
67	Member 6 Element 8 In Plane Strain
68	Member 6 Element 8 Extension Strain
69	Member 6 Element 9 Twist Strain
70	Member 6 Element 9 Out of Plane Strain
71	Member 6 Element 9 In Plane Strain
72	Member 6 Element 9 Extension Strain
73	Member 5 Element 1 Twist Strain
74	Member 5 Element 1 Out of Plane Strain Rates
75	Member 5 Element 1 In Plane Strain Rates
76	Member 5 Element 1 Extension Strain Rates
77	Member 5 Element 2 Twist Strain Rates
78	Member 5 Element 2 Out of Plane Strain Rates
79	Member 5 Element 2 Extension Strain Rates

Table A.3: States for Flexible Model (cont.)

State Number	Contribution
80	Member 5 Element 2 Twist Strain Rates
81	Member 5 Element 3 Out of Plane Strain Rates
82	Member 5 Element 3 In Plane Strain Rates
83	Member 5 Element 3 Extension Strain Rates
84	Member 5 Element 3 Twist Strain Rates
85	Member 5 Element 4 Out of Plane Strain Rates
86	Member 5 Element 4 In Plane Strain Rates
87	Member 5 Element 4 Extension Strain Rates
88	Member 5 Element 4 Twist Strain Rates
89	Member 5 Element 5 Out of Plane Strain Rates
90	Member 5 Element 5 In Plane Strain Rates
91	Member 5 Element 5 Extension Strain Rates
92	Member 5 Element 5 Twist Strain Rates
93	Member 5 Element 6 Out of Plane Strain Rates
94	Member 5 Element 6 In Plane Strain Rates
95	Member 5 Element 6 Extension Strain Rates
96	Member 5 Element 6 Twist Strain Rates
97	Member 5 Element 7 Out of Plane Strain Rates
98	Member 5 Element 7 In Plane Strain Rates
99	Member 5 Element 7 Extension Strain Rates
100	Member 5 Element 7 Twist Strain Rates
101	Member 5 Element8 Out of Plane Strain Rates
102	Member 5 Element 8 In Plane Strain Rates
103	Member 5 Element 8 Extension Strain Rates
104	Member 5 Element 8 Twist Strain Rates
105	Member 5 Element 9 Out of Plane Strain Rates
106	Member 5 Element 9 In Plane Strain Rates
107	Member 5 Element 9 Extension Strain Rates
108	Member 5 Element 9 Twist Strain Rates
109	Member 6 Element 1 Out of Plane Strain Rates
110	Member 6 Element 1 In Plane Strain Rates
111	Member 6 Element 1 Extension Strain Rates
112	Member 6 Element 1 Twist Strain Rates
113	Member 6 Element 2 Out of Plane Strain Rates
114	Member 6 Element 2 In Plane Strain Rates
115	Member 6 Element 2 Extension Strain Rates
116	Member 6 Element 2 Twist Strain Rates
117	Member 6 Element 3 Out of Plane Strain Rates
118	Member 6 Element 3 Extension Strain Rates
119	Member 6 Element 3 Twist Strain Rates

Table A.4: States for Flexible Model (cont.)

State Number	Contribution
120	Member 6 Element 3 Out of Plane Strain Rates
121	Member 6 Element 4 In Plane Strain Rates
122	Member 6 Element 4 Extension Strain Rates
123	Member 6 Element 4 Twist Strain Rates
124	Member 6 Element 4 Out of Plane Strain Rates
125	Member 6 Element 5 In Plane Strain Rates
126	Member 6 Element 5 Extension Strain Rates
127	Member 6 Element 5 Twist Strain Rates
128	Member 6 Element 5 Out of Plane Strain Rates
129	Member 6 Element 6 In Plane Strain Rates
130	Member 6 Element 6 Extension Strain Rates
131	Member 6 Element 6 Twist Strain Rates
132	Member 6 Element 6 Out of Plane Strain Rates
133	Member 6 Element 7 In Plane Strain Rates
134	Member 6 Element 7 Extension Strain Rates
135	Member 6 Element 7 Twist Strain Rates
136	Member 6 Element 7 Out of Plane Strain Rates
137	Member 6 Element8 Extension Strain Rates
138	Member 6 Element 8 Twist Strain Rates
139	Member 6 Element 8 Out of Plane Strain Rates
140	Member 6 Element 8 In Plane Strain Rates
141	Member 6 Element 9 Extension Strain Rates
142	Member 6 Element 9 Twist Strain Rates
143	Member 6 Element 9 Out of Plane Strain Rates
144	Member 6 Element 9 In Plane Strain Rates
145	Member 6 V_x
146	Member 6 V_y
147	Member 6 V_z
148	Member 6 w_x
149	Member 6 w_y
150	Member 6 w_z
151	Member 6 Yaw
152	Member 6 Pitch
153	Member 6 Roll

Bibliography

1. Blake, William B. "UAV Aerial Refueling- Wind Tunnel Results and Comparison with Analytical Prediction". (AIAA 2004-4820), 2004.

2. Brown, E. L. *Integrated Strain Actuation in Aircraft with Highly Flexible Composite Wings*. Ph.D. thesis, Massachusetts Institute of Technology, Boston, Massachusetts, June 2003. PhD Dissertation.

3. Dogan, Atilla, Sriram Venkataramanan, and William Blake. "Modeling of Aerodymanic Coupling Betweeen Aircraft in Close Proximity". *Journal of Aircraft*, (Volume 42 Number 4):120–130, 2005.

4. Nalepka, Joseph P. and Jacob L. Hinchman. "Automated Aerial Refueling: Extending the Effectiveness of Unmanned Air Vehicles". (AIAA 2005-6005), 2005.

5. Patil, Mayuresh J., Dewey H. Hodges, and Carlos E.S. Cesnik. "Nonlinear Aeroelastic Analysis of Complete Aircraft in Subsonic Flow". *Journal of Aircraft*, (Volume 37 Number 5):87–92, September-October 2000.

6. Peters, D and A. Cao. "Finite State Induced Flow Models Part I : Two Dimentional Thin Airfoil". *Journal of Aircraft*, (Volume 32 Number 2), March-April 1995.

7. Peters, D and M.J Johnson. "Finite State Airloads for Deformable Airloads on Fixed and Rotating Wings". *Aeroelasticity and Fluid/Structure Interaction, Procedings of the Winter Annual Meeting*, November 6-11.

8. van Schoor, Marthinis C and Andreas H. von Flotow. "Aeroelastic Chracteristics of Highly Flexible Aircraft". *Journal of Aircraft*, (Volume 27 Number 10):17–26, October 1990.

9. Shearer, Christopher M. "Coupled Nonlinear Flight Dynamics, Aeroelasticity, and Control of Very Flexible Aircraft". 2006.

10. Shearer, Christopher M. and Carlos E.S. Cesnik. "NonLinear Flight Dynamics of Very Flexible Aircraft". San Fransisco, CA, August 15 - 18 2005. AIAA Paper No. 2005-5805, also J. Aircraft, 2007 (to appear).

11. Stevens, Brian L. and Frank L. Lewis. *Aircraft Control and Simulation*. John Wiley & Sons, Hoboken, NJ, second edition, 2003.

REPORT DOCUMENTATION PAGE

Form Approved
OMB No. 074-0188

1. REPORT DATE *(DD-MM-YYYY)*	2. REPORT TYPE	3. DATES COVERED *(From – To)*
13 September 2007	**Thesis**	Sep 2006 – Sep 2007

4. TITLE AND SUBTITLE
Flight Dynamic Response of HALE Aircraft to KC-135 Flowfield

5a. CONTRACT NUMBER

5b. GRANT NUMBER

5c. PROGRAM ELEMENT NUMBER

6. AUTHOR(S)

Amanda J Devuono

5d. PROJECT NUMBER

5e. TASK NUMBER

5f. WORK UNIT NUMBER

7. PERFORMING ORGANIZATION NAMES(S) AND ADDRESS(S)

Air Force Institute of Technology
Graduate School of Engineering and Management (AFIT/ENY)
2950 Hobson Way
WPAFB OH 45433-7765

8. PERFORMING ORGANIZATION REPORT NUMBER

AFIT/GAE/ENY/07-S06

9. SPONSORING/MONITORING AGENCY NAME(S) AND ADDRESS(ES)

10. SPONSOR/MONITOR'S ACRONYM(S)

11. SPONSOR/MONITOR'S REPORT NUMBER(S)

12. DISTRIBUTION/AVAILABILITY STATEMENT
APPROVED FOR PUBLIC RELEASE; DISTRIBUTION UNLIMITED.

13. SUPPLEMENTARY NOTES

14. ABSTRACT This research effort examines the static affects of a KC-135 flowfield on a flexible winged Sensorcraft model. The KC-135 flowfield data is generated by a vortex lattice code and integrated into Sensorcraft model for analysis. Building on previous research, a refueling situation was modeled to note the effects of the Sensorcraft at varying locations within the flowfield. The Sensorcraft model was analyzed for both rigid and flexible wings as a means of comparision. Flowfield locations of interest were determined and trimmed conditions were computed for each flowfield location. Utilizing the trimmed condition and flowfield locations, the nonlinear set of EOM's were linearized in order to complete an eigenvalue/eigenvector analysis. Unstable eigenvalues were found for the rigid and flexible cases at all flowfield locations, and the specific contributions to the states were noted and classified accordingly. Results indicate that when the Sensorcraft was moved to different locations, the number and magnitude of the unstable eigenvalues fluctuated. Areas of the flowfield with increases in unstable eigenvalues were determined to be where the Sensorcraft experienced asymmetric loading, primarily when offset from the centerline of the flowfield. The additional elastic states for the flexible winged cases showed a significant increase in unstable eigenvalues.

15. SUBJECT TERMS
Aircraft, flexible coupling, thin wings, flowfields

16. SECURITY CLASSIFICATION OF: unclassified			17. LIMITATION OF ABSTRACT	18. NUMBER OF PAGES	19a. NAME OF RESPONSIBLE PERSON
a. REPORT					Christopher Shearer, Maj, USAF (ENY)
U	**U**	**U**	**UU**	79	**19b. TELEPHONE NUMBER** *(Include area code)* 937-255-3636 x4587